This is a preprint, the final version is subject to change, of the American Mineralogist (MSA)
Cite as Authors (Year) Title. American Mineralogist, in press.
(DOI will not work until issue is live.) DOI: http://dx.doi.org/10.2138/am-2016-5127

Hafnium, oxygen, neodymium, strontium, and lead isotopic constraints on magmatic evolution of the supereruptive southern Black Mountains volcanic center, Arizona, USA: A combined LASS zircon - whole-rock study

(Revison 2c)

Susanne M. McDowell[1,2], Sarah Overton[3], Christopher M. Fisher[4], William O. Frazier[1], Calvin F. Miller[1], Jonathan S. Miller[3], and Rita C. Economos[5]*

[1]Vanderbilt University, Earth and Environmental Sciences
PMB 351805, 2301 Vanderbilt Place, Nashville, TN 37235-1805

[2]Hanover College, Department of Geology
484 Ball Drive, Hanover, IN 47243

[3]San Jose State University, Geology Department
One Washington Square, San Jose, CA 95192

[4]Washington State University, School of the Environment
PO Box 642812, Pullman WA 99164-2812

[5]University of California – Los Angeles, Department of Earth and Space Sciences
595 Charles Young Drive East, P.O. Box 951567, Los Angeles, CA 90095*

*Current address: Southern Methodist University, Roy M. Huffington Department of Earth Sciences, 3225 Daniel Avenue, Dallas, TX 75205

Abstract

The >700 km3 Peach Spring Tuff (PST), erupted at 18.8 Ma from the Silver Creek caldera in the southern Black Mountains volcanic center (SBMVC) of western Arizona, is the only supereeruption-scale ignimbrite in the northern Colorado River Extensional Corridor. The SBMVC contains pre- and post-caldera volcanic rocks and caldera-related intrusions (~19–17 Ma) that provide a detailed petrologic record of ignimbrite antecedence and aftermath.

Whole-rock Sr-Nd-Pb-Hf isotopic data combined with complementary zircon O and Hf isotopic data from a suite of pre- through post-PST samples provide robust constraints on (1) how the SBMVC evolved with respect to magmatic sources and processes throughout its ~2 Ma history and (2) the petrogenetic relationships between the PST and slightly younger intracaldera plutons. Both pre- and post-PST units have isotopic ranges (ε_{Nd} = -8.3 to -11.6, ε_{Hf} = -8.2 to -14.0, $^{87}Sr/^{86}Sr_i$ = 0.709-0.712; $^{206}Pb/^{204}Pb$ = 18.19-18.49, $^{207}Pb/^{204}Pb$ = 15.60-15.62, $^{208}Pb/^{204}Pb$ = 38.95-39.29) that fall within the spectrum of Miocene Colorado River Extensional Corridor rocks and are consistent with mixing of substantial fractions of Proterozoic (Mojave) crust and juvenile material derived from regional enriched mantle. Compared to the PST, which has relatively uniform isotopic ratios (ε_{Nd} = -11.4 to -11.7, ε_{Hf} = -13.8 to -14.3, $^{87}Sr/^{86}Sr_i$ = 0.709-0.712; $^{206}Pb/^{204}Pb$ = 18.20-18.29, $^{207}Pb/^{204}Pb$ = 15.60-15.62, $^{208}Pb/^{204}Pb$ = 39.02-39.33), individual pre- and post-PST units are isotopically more variable and generally more primitive.

Consistent with whole-rock isotopes, zircon ε_{Hf} (-8 to -14) and oxygen $\delta^{18}O$ (+4.5 to +7.2 ‰) for most pre- and post-PST units also have wider ranges and more mantle-like values than those of the PST (-12 to -15, +6.1 to +7.1‰). Moreover, zircon isotopic compositions decrease in post-PST samples. Afew zircons from post-PST intrusions have $\delta^{18}O$ values lower than mantle values,(<+5‰), suggesting incorporation of hydrothermally altered rock.

Whole-rock and zircon elemental and isotopic analyses indicate that (1) most pre- and post-PST units are less evolved and less homogenized than the PST itself; (2) intrusions in the Silver Creek caldera are petrogenetically distinct from the PST and therefore represent discrete magmatic pulses, not unerupted PST mush; (3) enriched mantle input increased in the SBMVC following the paroxysmal PST eruption; (4) post-PST history of the SBMVC was characterized by periodic influx of magmas with varying juvenile fractions into pre-existing mushy or solidified intrusions, resulting in variable and incomplete hybridization; and (5) melting and assimilation of hydrothermally-altered crust played a relatively minor role in the generation and evolution of magmas in the SBMVC.

Keywords: volcanic center, petrogenesis, zircon, oxygen isotopes, Sr isotopes, Hf isotopes, Nd isotopes, Pb isotopes, supereruption

Introduction

The southern Black Mountains volcanic center (SBMVC), located in the northern Colorado River Extensional Corridor (CREC) of northwestern Arizona, comprises the >700 km^3 Peach Spring Tuff (PST); its source, the Silver Creek caldera; and well-exposed pre- to post-PST volcanic units and intracaldera intrusions that were emplaced over a period of 2 m.y. (Ferguson et al., 2013; Pamukcu et al., 2013; McDowell et al., 2014). The completeness of the SBMVC's magmatic record and the recent finding that the age of part of the intracaldera intrusion complex is indistinguishable from that of the PST (McDowell et al., 2014) make it an attractive locality for exploring two questions that have attracted widespread interest: (1) How do volcanic centers that produce large-volume explosive eruptions evolve with respect to magmatic source(s), composition, and processes (e.g., Lipman, 2007; Tappa et al., 2011; Watts et al., 2011, 2012)? (2) What are the petrogenetic relationships between volcanic rocks and spatially associated subvolcanic intrusions (e.g., Bachmann & Bergantz, 2004; Bachmann et al., 2007; Glazner et al., 2008)? More specifically, what are the relationships between very large ignimbrites and the ~contemporaneous plutons in their source calderas (e.g., Lipman, 1984; Bachmann & Bergantz, 2008; Zimmerer & McIntosh, 2012a, b; Mills & Coleman, 2013)? In the case of the SBMVC, are the intracaldera intrusions unerupted remnants of supereruption magmas, or do they represent discrete magmatic pulses?

To address these questions with respect to the SBMVC, we apply a combination of whole-rock Sr-Nd-Hf-Pb and *in situ* zircon O and Hf isotopic analysis. Because isotopes of Sr, Nd, Pb, and Hf are not appreciably fractionated as a consequence of closed-system processes, their ratios remain effectively constant in the products of closed-system crystallization and melt segregation on the time scales involved. Only open-system events, like magma mixing and crustal assimilation, can create isotopic variability within a magma. Moreover, radiogenic isotopic ratios constrain source composition and age. Previous studies have shown that Proterozoic, Mesozoic, and Miocene-age rocks in the Mojave Desert region, which includes the SBMVC, have distinctive Sr, Nd, and Pb isotopic signatures (e.g., Bennett & DePaolo, 1987; Farmer et al., 1989; Wooden & Miller, 1990; Feuerbach et al., 1993; Miller & Wooden, 1994; Falkner et al., 1995; Metcalf et al., 1995; Miller et al., 2000; Bachl et al., 2001; Ericksen et al., 2004). The isotopic characteristics established by these studies serve as regional benchmarks against which we can compare the isotopic compositions of the SBMVC and with which we can constrain sources and open-system processes such as assimilation and magma mixing.

The introduction of high-precision, high-resolution analytical techniques has permitted determination of isotopic ratios *in situ* in minerals. Hafnium and oxygen isotopic compositions of zircons offer particularly valuable insights into magmatic origins and evolution. More sensitively than whole-rock analyses, *in situ* Hf isotope data provide constraints on magmatic sources, degree of magmatic heterogeneity, and open-system processes (e.g., Hawkesworth & Kemp, 2006; Kemp et al., 2006, 2007; Kemp et al., 2010; Drew et al., 2013). Oxygen isotope ratios determined *in situ* in zircon shed complementary light on magmatic characteristics and processes; in particular, they document varying input from crustal materials that have interacted with surface water (e.g., Bindeman & Valley, 2001; Valley et al., 2005; Hawkesworth & Kemp, 2006; Bindeman et al., 2007; Kemp et al., 2007; Watts et al., 2011, 2012).

We combine our comprehensive isotopic data with new and existing whole-rock and zircon elemental data to characterize representative volcanic and intrusive units in the SBMVC. We then apply the constraints offered by the data set to investigate magmatic sources and processes and plutonic-volcanic connections.

Geological Context

The 70 to 100 km-wide northern Colorado River Extensional Corridor (CREC) is a zone of north-northwest-trending crustal blocks bounded by normal faults at the eastern edge of the Basin and Range in western Arizona, southern Nevada, and southeastern California (Fig. 1; Faulds et al., 1990, 2001). It formed between ~20 and 12 Ma when lithospheric extension, preceded and accompanied by intermediate to silicic magmatism, dismembered Proterozoic- and Mesozoic-age continental crust (Faulds et al., 1990, 2001; Varga et al., 2004). Evidence for the region's tectonic and volcanic upheaval during the middle Miocene is well preserved within the northern CREC as thick sequences (>3 km) of volcanic and sedimentary strata and dissected coeval plutons (e.g., Faulds, 1990; Falkner et al., 1995; Bachl et al., 2001; Miller & Miller, 2002; Metcalf, 2004; Walker et al., 2007; Lang et al., 2008).

The southern Black Mountains produced the most voluminous eruption in the northern CREC: the "supereruption" of the Peach Spring Tuff (PST) at 18.8 Ma (Lidzbarski et al., 2012; Ferguson et al., 2013; Pamukcu et al., 2013). The PST ignimbrite is widely recognized in southeastern California, southern Nevada, and western Arizona (Young & Brennan, 1974; Glazner et al., 1986; Buesch & Valentine, 1992) (Fig. 1a). Its source, the Silver Creek caldera, was dismembered during post-PST extension, with a smaller fragmented now exposed across the Colorado River in the Sacramento Mountains, California (Ferguson et al., 2013).

Although the PST represents by far the largest eruption in the southern Black Mountains, it was bracketed by ~2 million years of volcanic activity (Pearthree et al., 2010; McDowell et al., 2012; McDowell et al., 2014; Table 1). The Silver Creek caldera and its environs (Fig. 1) provide a temporal record of pre- to post-PST magmatism in the vicinity of the caldera (Lang, 2001; Lang et al., 2008; McDowell et al., 2014).

We define the SBMVC to encompass the exposures of igneous rocks that predate and immediately post-date the PST, in the southern Black Mountains where a thick pre-PST volcanic section is exposed (Fig. 1). The northern boundary of the SBMVC is near Union Pass, a zone identified by Murphy and Faulds (2003) and Murphy et al. (2004) as a "temporal domain boundary" between 19-17 Ma extension to the south and <16 Ma extension to the north (Fig. 1); it is also at or near the northernmost extent of thick, intermediate-composition pre-PST volcanic units (Faulds et al., 1995; Lang, 2001; Murphy et al., 2013). The western boundary is buried beneath Quaternary alluvium that fills the broad basin through which the Colorado River flows; Kingman, Arizona, where pre-PST trachyte is absent from the stratigraphic section, is at the eastern margin. The southern boundary is at the southernmost extent of the Black Mountains, approximately 20 km southeast of the Silver Creek caldera (Fig. 1).

Stages of SBMVC magmatism

We divide SBMVC magmatism into three stages based on this and previous studies (e.g., Lang et al., 2008; Pearthree et al., 2010; Pamukcu et al., 2013; McDowell et al., 2014): (1) initial, predominantly intermediate-composition, effusive volcanism; (2) the dominantly silicic PST eruption; and finally (3) compositionally-diverse, small-volume volcanism and epizonal intrusions (Fig. 2).

(1) Pre-PST magmatism is dominated by thick, phenocryst-rich (~10-40%, biotite and plagioclase) trachytic, trachydacitic, and trachyandesitic lavas that overlie Precambrian basement and are exposed from Union Pass to the southernmost Black Mountains (Fig. 1; Ransome, 1927; Thorson, 1971; DeWitt et al., 1986; Faulds et al., 1999; Lang, 2001; Murphy, 2004; Lang et al., 2008; Pearthree et al., 2010). These intermediate-composition lavas exceed ~1 km thickness throughout the southern 40 km of the Black Mountains, thinning to less than 200 m 15 km north of Silver Creek caldera (Fig. 1) (Lang et al., 2008; Ferguson et al., 2013; Murphy, 2004; Murphy et al., 2013). This suggests a total volume on the order of 10^3 km^3. Faulds et al. (1999) obtained biotite $^{40}Ar/^{39}Ar$ ages for pre-PST lava of 19.19 +/- 0.06 Ma and 19.59 +/- 0.03 Ma. CA-TIMS U-Pb dating of zircons extracted from Alcyone trachyte yielded a weighted mean age of 19.01 +/- 0.2 Ma (McDowell et al., 2014). The Alcyone trachyte comprises a thick sequence of lavas at the base of the pre-PST section (Ransome, 1927; Thorson, 1971; Dewitt et al., 1986). Units higher in the section include the Gold Road trachyte (Ransome, 1927; Thorson, 1971; Dewitt et al., 1986); thinner mafic to intermediate lavas including the Wrigley Mine basaltic trachyandesite and Esperanza trachyte (Pearthree et al., 2010), exposed to the southeast of the Silver Creek caldera and near Union Pass (Fig. 1, Pearthree et al., 2010; Ferguson et al., 2013; Murphy et al., 2013); and the Cook Canyon Tuff, an ignimbrite ranging from ~10-100 m in thickness that was produced by the largest explosive eruption in the SBMVC other than the PST (Buesch and Valentine, 1986; Murphy, 2004; Murphy et al., 2013).

(2) The PST consists of a >0.5 km-thick, phenocryst-rich intracaldera trachyte that fills Silver Creek caldera, and outflow that includes trachyte at the tops of some proximal exposures but is dominated by high-silica rhyolite (Pamukcu et al., 2013; Ferguson et al., 2013; Frazier, 2013). Outflow PST is exposed over an area of 32,000 km^2 (Fig. 1; Buesch, 1991; Ferguson et al., 2013). $^{40}Ar/^{39}Ar$ dating of PST sanidine yielded an age of 18.78 +/- 0.02 Ma (Ferguson et al., 2013); a correction of systematic bias using the algorithms of Renne et al. (2010, 2011) gives an older age of 18.84 ± 0.02 Ma (McDowell et al., 2014). Lidzbarski reports U-Pb zircon CA-

TIMS and CA-SIMS ages that are consistent with these results (Lidzbarski et al., 2012; Lidzbarski, 2014).

(3) Post-PST magmatism is represented by epizonal intrusions and small-volume lavas and tuffs:

Intrusions include two intra- and pericaldera stocks with a total area of exposure ~30 km^2, the Moss porphyry (mostly quartz monzodiorite and quartz monzonite) and the Times porphyry (granite), and compositionally diverse porphyry dikes and small plugs that are exposed both within the caldera and within a radius of 10 km (Ransome, 1923; Thorson, 1971; DeWitt et al., 1986; McDowell et al., 2014). Most dikes and plugs are silicic, but some dikes have intermediate compositions or are composite. The stocks intrude the PST and display clear evidence for magma mingling and likely hybridization, including magmatic enclaves and rounded, rimmed feldspars (McDowell et al., 2014). Magmatic enclaves and rounded phenocrysts of feldspar and quartz are also locally present in the intermediate and silicic dikes (McDowell et al., 2014). U-Pb CA-TIMS zircon ages for the Moss porphyry(18.76 ± 0.11 Ma and 18.84 ± 0.15 Ma) are within error of PST U-Pb zircon and Ar/Ar sanidine ages; Times porphyry and composite dikes that we interpret to be associated with the Moss and Times intrusions range from 18.7 to 18.5 Ma, and a large intracaldera dike is 18.2 Ma (McDowell et al., 2014, zircon CA-TIMS U-Pb).

Post-PST volcanic rocks in the southern Black Mountains consist of ~18.7 to 16.9 Ma intermediate to silicic ignimbrites, block-and-ash flow deposits, lava flows, and volcanogenic sediments (Fig. 1; Faulds et al., 1999; Murphy, 2004; Lang et al., 2008; Pearthree et al., 2010; Murphy et al., 2013; McIntosh & Ferguson, unpublished Ar ages). In this study we investigate two of these units: a prominent, glassy ~18.5 Ma silicic lava (McDowell et al., 2014) and its magmatic enclaves, and a 17.5 Ma intermediate-composition lava containing 2-3 cm euhedral feldspar phenocrysts (McIntosh & Ferguson, unpublished Ar ages).

Methods

Whole-rock Analysis

Elemental compositions: Analyses of 19 representative pre- and post-PST samples from the SBMVC were carried out by Activation Laboratories in Ancaster, Ontario, by INAA, ICP, and ICP-MS (Table 2). Fifteen of these were previously reported in McDowell et al. (2014). For this study, we sent four additional samples to Activation Laboratories and include these in Table 2. We also include analyses of ten PST samples for which we obtained whole-rock isotopic compositions (8 pumice and fiamme, 2 enclaves). A total of 33 elemental analyses of PST pumice and fiamme are plotted in Figure 2 (from Pamukcu et al., 2013, and Frazier, 2013).

Isotopic compositions: We determined whole-rock isotope compositions (Sr, Hf, Nd and Pb) for the same 19 samples as for elemental analysis, along with 8 PST pumice samples and two enclaves from PST, at the WSU Radiogenic Isotope and Geochronology Laboratory (RIGL) at Washington State University (Table 3). Approximately 0.25 g of each powdered sample were placed in Teflon vessels, dissolved in ~7 mL 10:1 HF:HNO_3, and immediately dried at 120 °C to eliminate silica. Samples were then redissolved in ~7 mL 10:1 HF:HNO_3 and placed in steel-jacketed Parr bombs at 150°C for 5-7 days. The solutions were dried down and redissolved overnight in a mixture of 6M HCl/H_3BO_3 to convert to chlorides and minimize the production of fluoride species. Samples were dried down again and redissolved in Parr bombs at 150°C for 24 hours in 6M HCl until sample solutions were clear. These solutions were dried yet again, then redissolved in a mixture of 1M HCl and 0.1M HF. High-field-strength elements (including Hf), REE (including Nd), and Sr were initially separated on single cation exchange columns loaded with AG 50W-X12 resin (200-400 mesh). Following the method of Patchett & Tatsumoto (1981), Hf was eluted at the beginning of the procedure in 1M HCl/0.1M HF, followed by elution of Sr in 2.5M HCl and finally bulk REE separation in 6M HCl. Ti was removed from the Hf fraction, a crucial step, as excess Ti has been shown to alter the measured Hf isotopic composition; Blichert-Toft et al., 1997. Any remaining Yb and Lu in the Hf aliquot were removed in a third stage of column chemistry using 0.18 mL of AG 50W-X12 resin. Sr aliquots were subsequently purified using 0.18 mL Sr-spec resin and HNO_3 (e.g., Gaschnig et al., 2011). Nd was separated from other REEs using LN Spec resin (Gaschnig et al., 2011).

To minimize Pb blanks, we dissolved additional aliquots of each sample specifically for Pb analysis and, following the approach of Prytulak et al. (2006), separated Pb from solution using Biorad AG1-X8 anion resin. Pb aliquots were then spiked with Tl, in order to correct for mass fractionation as described by Gaschnig et al. (2011).

Aliquots of each purified species (Sr, Nd, Hf, Pb) were redissolved in 2% HNO_3 for determination of isotopic compositions on the WSU Thermo-Finnigan Neptune MC-ICP-MS. Whole-rock Hf analyses were corrected for mass fractionation using $^{179}Hf/^{177}Hf = 0.7325$ and normalized using Hf standard JMC475 ($^{176}Hf/^{177}Hf = 0.282160$). Sr analyses were corrected for mass fractionation using $^{86}Sr/^{88}Sr = 0.1194$ and normalized using standard NBS-987 ($^{87}Sr/^{86}Sr = 0.710240$). Nd analyses were corrected for mass fractionation using $^{146}Nd/^{144}Nd = 0.7219$ and normalized using Nd standard Ames ($^{143}Nd/^{144}Nd = 0.512138$). We corrected for mass bias in the Pb analyses using $^{205}Tl/^{203}Tl = 2.388$ and normalized the mass bias corrected values for standard NBS 981 using $^{206}Pb/^{204}Pb = 16.9405$, $^{207}Pb/^{204}Pb = 15.4963$, $^{208}Pb/^{204}Pb = 36.7219$ (Galer &

Abouchami, 1998). ε_{Hf} and ε_{Nd} were calculated using the CHUR parameters reported by Bouvier et al. (2008).

In situ zircon analyses (oxygen and Lu-Hf)

We performed *in situ* oxygen isotope and Lu-Hf isotope measurements on zircon from representative pre- to post-PST units: five pre-PST volcanic samples, 13 intrusive post-PST samples, and three volcanic post-PST samples (Supplement tables 1,2). Zircon grains were separated from whole rock using standard methods, including crushing, density separation by water table and heavy liquids, magnetic susceptibility separation by Frantz magnetic separator, and hand-picking. Grains were then mounted in epoxy and polished to their approximate centers and imaged using SEM cathodoluminescence on the JEOL JSM 5600 scanning electron microscope (SEM) at the Microanalysis Center shared by the US Geological Survey and Stanford University.

Oxygen isotopes: Following the methods of Trail et al. (2007), we carried out a total of 467 O isotope analyses (93 pre-PST, 312 post-PST intrusive, 62 post-PST volcanic) at UCLA using the CAMECA IMS 1270 in multi-collection mode (Cs+ primary beam spot size ~20-25 microns). Analyses were calibrated using zircon standard R33, which yielded an in-run reproducibility of 0.48‰. $\delta^{18}O$ was calculated using VSMOW (Baertschi, 1976). Cited precisions are the geometric mean of the within-spot standard error and the in-run reproducibility on R33. The full data set is reported in Supplement appendix 2.

Lu-Hf isotopes: Following analyses for O isotopic composition, the mounts were lightly repolished and the age and Lu-Hf isotope composition was determined on a subset of the same grains at RIGL. We conducted a total of 239 analyses of four pre-PST samples (29 analyses), three PST samples (30 analyses), 12 post-PST intrusive samples (139 analyses), and three post-

PST volcanic samples (41 analyses).

Analyses were carried out using the laser ablation split-stream method (LASS) whereby U-Pb age and Lu-Hf isotope composition are determined simultaneously (Fisher et al., 2014a). The LASS approach is critical in zircon samples having multiple age components present within single grains, as it allows detection of inadvertent incorporation of ancient zircon domains when targeting younger (i.e., Miocene age) domains (Fisher et al., 2014a, Fisher et al., 2014b). Given the young age, and thus low very low radiogenic Pb concentrations, relatively large analytical uncertainties exist for age determinations, and thus we prefer the higher precision SIMS age (McDowell et al., 2014). Hf isotope measurements that yielded concurrently-measured mixed U-Pb ages (i.e., discordant) are excluded from Figs. 4 and 5.

In order to constrain the age and Hf isotope composition of the source materials, a small subset of analyses targeted inherited cores (Table 4). When possible, we selected ablation sites that overlapped with previous O isotope analysis locations. Care was taken to avoid placing the laser beam over multiple CL zones. Analyses were calibrated using zircon standards R33 and FC1. The mean $^{176}Hf/^{177}Hf$ for R33 and FC1 (0.282181 ± 36 (2SD), n= 73; 0.282754 ± 42 (2SD), n= 112) are in close agreement with the solution MC-ICPMS values of 0.282184 ± (Woodhead and Hergt, 2005) and 0.282764 ± 14 (Fisher et al., 2014). Reference zircons 91500 and GJ-1 were analyzed as secondary standards for both U-Pb age and Lu-Hf isotopic composition and are in good agreement with published reference values. Eleven LASS analyses of 91500 yielded a weighted mean $^{206}Pb/^{238}U$ age of 1068 ± 12 Ma (2SE) and a mean $^{176}Hf/^{177}Hf$ of 0.282293 ± 37 (2SD) (Schoene et al., 2006; Blichert-Toft, 2008), while 10 LASS analyses of GJ-1 yielded a weighted mean $^{206}Pb/^{238}U$ age of 596 ± 9 Ma (2SE) and a mean $^{176}Hf/^{177}Hf$ of 0.282015 ± 35 (2SD) (Morel et al., 2008). Analyses of all reference materials are reported in detail in Supplement Appendix 3. ε_{Hf} was calculated using CHUR parameters reported by Bouvier et al. (2008). External 2-sigma precision was ≤ 1.5 ε_{Hf}.

The full data set is reported in Supplement appendix 1.

Results

Whole-rock geochemistry documents SBMVC magmatic evolution from predominantly intermediate-composition effusive volcanism (pre-PST), to a high-volume high-silica explosive event (PST), and finally to compositionally diverse volcanic and intrusive magmatism (post-PST). Pre-PST volcanic rocks have 48 to 70 wt% SiO_2; post-PST intrusions, 55 to 80 wt%; and post-PST volcanic rocks, 48 to 75 wt% (Lang et al., 2008; Pearthree et al., 2010; Frazier, 2013; McDowell et al., 2014; Fig. 2; Tables 1, 2). True mafic rocks (basalts and gabbros) are relatively rare, and, except for PST, Times porphyry, and minor dikes and stocks, rhyolites and granites are also uncommon. The dominant SBMVC intermediate rocks are rich in total alkalis and especially in K_2O and almost all are basaltic trachyandesite, trachyandesite, and trachydacite or trachyte in the classification scheme of Le Bas et al. (1986). Most samples fall in the trachyte plus trachydacite field and are trachytes according to the criterion normative Qz/(Qz+Pl+Or) <0.2, and therefore for simplicity we use the term "trachyte" as a general descriptor. Pre- and post-PST units are elementally distinct from the PST, which has lower Sr and Ba and higher Zr and Rb at a given SiO_2 than its magmatic predecessors and successors (Fig. 2).

Sr, Nd, and Hf isotopic ranges for pre-PST units ($^{87}Sr/^{86}Sr_i$ = 0.7093 to 0.7110, ε_{Nd} = -8.3 to -11.6, and ε_{Hf} = -8.2 to -14.0) are similar to those of post-PST volcanics and intrusions ($^{87}Sr/^{86}Sr_i$ = 0.7091 to 0.7124, ε_{Nd} = -8.4 to -10.4, and ε_{Hf} = -8.8 to -13.1) (Table 3, Fig. 3). Times and Moss magmatic enclaves (SCM-27b and MPe1, respectively) have the most primitive isotopic ratios (e.g., highest ε_{Hf} and ε_{Nd}). Throughout the sample suite, ε_{Nd} shows a strong positive correlation with ε_{Hf}. All pre- and post-PST units have Pb isotopic ratios within the ranges $^{206}Pb/^{204}Pb$ = 18.19-18.49, $^{207}Pb/^{204}Pb$ = 15.60-15.62, and $^{208}Pb/^{204}Pb$ = 38.95-39.29. PST samples are more uniform isotopically and generally have lower ε_{Nd} and ε_{Hf} and higher $^{87}Sr/^{86}Sr_i$ than the other SBMVC rocks ($^{87}Sr/^{86}Sr_i$ = 0.7108 to 0.7121 (with one higher outlier, see discussion), ε_{Nd} = -11.4 to -11.6, and ε_{Hf} = -13.8 to -14.2); Pb isotope ratios are similar to those of the rest of the SBMVC ($^{206}Pb/^{204}Pb$ = 18.20-18.29, $^{207}Pb/^{204}Pb$ = 15.60-15.62, and $^{208}Pb/^{204}Pb$ = 39.09-39.32). Collectively, SBMVC units have isotopic signatures consistent with those determined for other Miocene intrusive and volcanic units within the northern CREC (e.g., Wooden & Miller, 1994; Metcalf et al., 1995; Falkner at al., 1995; Miller et al., 2000; Bachl et al., 2001; Ericksen et al., 2004) (Fig. 3).

Zircon $\delta^{18}O$ in the majority of pre-PST, PST, and post-PST units falls within the range +5 – +7.3‰, with several higher outliers between $\delta^{18}O$ = +7.8 to +8.8 (one extreme outlier has $\delta^{18}O$ = +12.2) and lower outliers between +4.2 to +5.0 (Fig. 4). Broadly, zircon $\delta^{18}O$ decreases from older to younger units: average $\delta^{18}O$ = +6.8 in the oldest sample, ~19 Ma Alcyone trachyte, whereas average $\delta^{18}O$ = +5.6 in the youngest samples, ~18.2 Ma silicic porphyry dikes (Fig. 4). PST values, excluding one lower outlier at 4.5‰, range from 5.6 and 7.2‰ and average 6.4‰.

The 239 LASS zircon spots interpreted to be of Miocene age yielded ε_{Hf} values that range from -6 to -16 (Fig. 4). Overall, ε_{Hf} is higher in post-PST units than in pre-PST units. The oldest sample, Alcyone trachyte, and the PST have the lowest values (near -14). All samples younger than PST have some zircons with ε_{Hf} >-10, whereas all analyzed zircons from PST or pre-PST units have ε_{Hf} <-10.

Six LASS analyses of zircons from five samples clearly reveal inheriteance: their $^{206}Pb/^{238}U$

and $^{207}Pb/^{206}Pb$ ages are 1.51-1.62 Ga and 1.66-1.75 Ga, respectively, and ε_{Hf} values are -30 to -34 (Table 4).

For most paired O and Hf analyses, obtained from the same areas of single zircon grains, ε_{Hf} correlates negatively with $\delta^{18}O$ (Table 5; Fig. 5a). This correlation breaks down for zircons with the lowest, near- and sub-mantle, $\delta^{18}O$ (<5.5‰). All of the low- $\delta^{18}O$ zircon analyses are from post-PST intrusive units, with exception of the single outlier PST grain.

Ranges of measured ε_{Hf} values in individual samples (excluding analyses that we interpret to have partly or entirely encountered inherited cores) are 3 to 7 units, in many cases exceeding ±2σ analytical uncertainty. Similarly, $\delta^{18}O$ displays one- to four-unit intrasample variation, also commonly exceeding analytical uncertainty (see Fig. 5b).

Discussion

Whole-rock Sr-Nd-Hf-Pb Isotopes

Whole-rock isotopic ratios serve to constrain contributions from potential sources for Miocene magmas in the CREC (Figure 3). The Proterozoic crust of this region is characterized by high to very high $^{87}Sr/^{86}Sr$ (>0.710, up to 0.80 and higher) and low to very low ε_{Nd} (~-15 to -22); Paleoproterozoic rocks in general, especially the more silicic rocks, are concentrated in the upper and lower portions of these ranges of values, respectively, whereas Mesoproterozoic rocks fall in the lower and upper portions (Bennett and DePaolo, 1987; Miller and Wooden, 1994). We are unaware of published whole-rock Hf isotope data for Proterozoic rocks in this area, but, based on the ε_{Nd}- ε_{Hf} correlations of the Crustal and Terrestrial Arrays (Vervoort et al., 1999, 2011) and present day ε_{Nd} of Proterozoic rocks in and near the CREC, we estimate that their ε_{Hf} values range from ~-17 to -33 Numerous studies have concluded that juvenile, mantle-derived magmas in the CREC and environs older than ~12 Ma, were derived from ancient enriched lithospheric mantle (ε_{Nd} <~4, $^{87}Sr/^{86}Sr$ >~0.705; e.g., Daley and DePaolo, 1992; DePaolo and Daley, 2000; Feuerbach et al., 1993; Metcalf et al., 1995 (also see Metcalf et al. op. cit. for a rare exception)). More silicic igneous rocks of Mesozoic and Cenozoic age span the Nd-Sr, and presumably Hf, isotopic range between what is thought to be the enriched regional lithospheric mantle and Proterozoic crust (Fig. 3) and are generally interpreted to reflect hybridization processes involving these two sources (e.g. Miller and Wooden, 1994; Allen et al., 1995; Bachl et al., 2001).

Lead isotope ratios for almost all mid-Miocene and older rocks in this region fall above the Northern Hemisphere Regression Line (elevated $^{207}Pb/^{204}Pb$ and $^{208}Pb/^{204}Pb$ relative to $^{206}Pb/^{204}Pb$). Wooden and coworkers (Wooden et al., 1988; Wooden & Miller, 1990; see also Feuerbach et al., 1998) have identified two Pb isotopic provinces: the Mojave province to the west is characterized by higher $^{207}Pb/^{204}Pb$ and $^{208}Pb/^{204}Pb$ than the Arizona province (Fig. 3). The boundary between the two provinces is thought to lie within the CREC, very near the SBMVC.

Sr_i and Nd isotope ratios for SBMVC samples overlap with those of other Miocene units within the CREC ($Sr_i \approx 0.709$ to 0.714, $\varepsilon_{Nd} \approx$ -8 to -15) (Fig. 3d). Like other CREC igneous units, isotopic signatures of SBMVC volcanics and intrusions suggest that they are mixtures of juvenile and crustal components, derived respectively from the regional enriched lithospheric mantle and the Proterozoic crust. The wide range of isotopic compositions implies a wide range of proportions of the two types of contributing materials. The less evolved compositions (lower Sr_i higher ε_{Nd}) permit a very high proportion of juvenile material, but the range of suggested compositions of purely juvenile magmas leaves unclear whether the less isotopically-evolved

SBMVC rocks could be derived entirely from the mantle or have a substantial crustal component. A great majority of analyzed samples lie in a swath between plausible mantle and crustal sources, which we interpret to indicate hybridization involving large, varying crustal and mantle fractions. Isotopic data for Mesozoic igneous units in and near the CREC overlap with those of the SBMVC (e.g., Miller & Wooden, 1994; Gerber et al., 1995) and could therefore represent plausible crustal sources that do not require hybridization with juvenile material. However, because the southern Black Mountains lack exposures of Mesozoic rocks, and extensive zircon dating has found no evidence of Mesozoic inheritance (McDowell et al., 2014; Lidzbarski et al., 2012, Lidzbarski, 2014; this study), we infer that Mesozoic-age crust did not serve as a significant contributor to SBMVC magmas.

Lead isotope ratios strongly suggest that SBMVC magmas were derived from the regional lithosphere (crust and mantle). More specifically, uniformly high $^{207}Pb/^{204}Pb$ and $^{208}Pb/^{204}Pb$ indicate origin within Mojave, not Arizona, province lithosphere (Fig. 3).

The PST, including both trachyte and rhyolite, and Alcyone trachyte have isotopic compositions that suggest the largest Paleoroterozoic crustal components among all sampled units. One outflow PST rhyolite pumice has much higher Sr_i of 0.723; this sample, like other PST rhyolites, has very low Sr concentration (17 ppm), and we attribute the high Sr_i to slight contamination through incorporation of a few percent of Proterozoic crust with much higher $^{87}Sr/^{86}Sr$ and Sr concentration (Miller and Wooden, 1994), perhaps as a lithic fragment. Other pre- and post-PST extrusive and intrusive units display a wider range of whole-rock isotopic values and have more primitive isotopic compositions on average (Fig. 3). Lower-SiO_2 units – particularly pre-PST lavas PSK-14 and PST-11, and post-PST magmatic enclaves in the Times and Moss porphyries and silicic lava SIT-1 – appear to have the largest juvenile component, with relatively high ε_{Nd} and ε_{Hf} and low $^{87}Sr/^{86}Sr_i$. Higher-SiO_2 units have lower ε_{Nd} and ε_{Hf}, and higher $^{87}Sr/^{86}Sr_i$ (Fig. 3).

The isotopic differences between the PST and all other SBMVC units except the Alcyone trachyte suggests that it, and perhaps the Alcyone as well, were petrogenetically distinct magmas. Notably, the intracaldera stocks and cross-cutting dikes have a similar range of compositions to the remainder of pre- and post-PST units but do not overlap with the PST.or the Alcyone sample

Zircon O and Hf Isotopes

To our knowledge there are no published Hf isotope data for zircons or whole rocks representing the Proterozoic crust or young mafic rocks interpreted to be juvenile in the CREC region. Based on ε_{Nd} thought to represent the juvenile enriched lithospheric mantle (Fig. 3) and the terrestrial ε_{Nd} and ε_{Hf} array (Vervoort et al., 1999, 2011), we estimate that juvenile ε_{Hf} in the CREC is roughly -2 to -8. As discussed above, we estimate that Miocene ε_{Hf} in the Proterozoic Mojave crust is roughly in the range -17 to -33. An alternative estimate for Miocene ε_{Hf} of Paleoproterozoic rocks, based on the calculated $^{176}Hf/^{177}Hf$ of the six Paleoproterozoic zircons in our data set and typical $^{176}Lu/^{177}Hf$ of crustal rocks (~0.0125), falls toward the lower end of that range (-16.4 to -20.4). Based upon these estimates, our zircon ε_{Hf} data are consistent with whole-rock data in suggesting that magmatic sources comprised both ancient crustal and juvenile mantle-derived material (Fig. 4; Table 5),with the highest values of ~-6 possibly representing growth from entirely juvenile magma and all others indicating highly variable amounts of hybridization.

Oxygen isotopic compositions of zircon are mostly >~5.6, somewhat heavier than expected for crystals grown from juvenile, mantle-derived magmas but mostly toward the lower end of the typical crustal zircon range. Thus further supports the inference that SBMVC magmas were hybrids that combined substantial proportions of juvenile mantle-derived and crustal components. The paucity of $\delta^{18}O$ values >+7 to +8‰ (Fig. 4; Supplement appendix 2) suggests limited input from metasedimentary sources (e.g. the abundant paragneisses of the Mojave terrane). A few relatively low $\delta^{18}O$ analyses ($\delta^{18}O$ = +4-5‰) from a silicic porphyry dike and Times porphyry zircons may reflect limited melting and assimilation of hydrothermally-altered rock during the SBMVC's post-PST magmatic stage (e.g., Bindeman & Valley, 2001), but the dearth of these values suggests that, unlike the large-volume continental magmatic centers along the Yellowstone-Snake River Plain trend (Bindeman & Valley, 2001; Watts et al., 2011; Drew et al., 2013), this process played a relatively minor role in the development and evolution of the PST and other SBMVC magmas.

Increasing average $\varepsilon_{Hf\text{-}Zircon}$ and decreasing $\delta^{18}O_{Zircon}$ in post-PST units is broadly consistent with whole-rock isotopic data that indicate increasing input of mantle-derived material into the SBMVC system after the PST eruption. This inference is supported by the relative abundance of post-PST zircons with enriched Mojave mantle-like zircon isotopic compositions (Fig. 5a).

Zircons from PST samples and the Alcyone trachyte have similar narrow ranges of relatively high $\delta^{18}O$ and low ε_{Hf} values, consistent with crystallization within an isotopically homogeneous magma body with a relatively large ancient crustal component. In contrast, zircons from most pre- and post-PST units and individual samples have wider isotopic ranges, lower average $\delta^{18}O$, and higher average ε_{Hf} (Fig. 4, 5). These characteristics indicate crystallization from petrogenetically diverse magmas with greater contributions from juvenile sources than PST, or Alcyone trachyte. The large ranges in $\delta^{18}O$ and ε_{Hf} in zircon from many samples, in many cases

This is a preprint, the final version is subject to change, of the American Mineralogist (MSA)
Cite as Authors (Year) Title. American Mineralogist, in press.
(DOI will not work until issue is live.) DOI: http://dx.doi.org/10.2138/am-2016-5127 10/21

beyond analytical uncertainty (see Supplement appendix 3), demonstrate isotopic disequilibrium. This indicates open-system processes whereby zircons crystallized in isotopically distinct melts prior to mingling and mixing (cf. McDowell et al., 2014).

Like the whole-rock data, zircon isotopic compositions reveal a petrogenetic distinction between the PST and intrusions. Moss porphyry zircon ages are within error of PST age (McDowell et al., 2014), but the two units are isotopically distinct: the Moss porphyry displays a greater range in $\delta^{18}O$ and ε_{Hf} than the PST and has a distinctly higher $\varepsilon_{Hf\text{-}WR}$, $\varepsilon_{Nd\text{-}WR}$, and average $\varepsilon_{Hf\text{-}Zircon}$; the Times porphyry and the dikes exhibit broadly similar averages and trends to those of the Moss porphyry. Thus, whereas effective isotopic homogenization of the PST magma body occurred prior to zircon saturation and crystallization (Frazier, 2013), isotopic variability in zircons from the intrusions document mingling and mixing that is also clearly revealed in outcrop and thin section, for example by quenched mafic enclaves and resorbed and rimmed crystals (McDowell et al, 2014).

Integration of zircon and whole-rock Hf isotope data

Comparison and integration of zircon and whole-rock ε_{Hf} offers constraints on SBMVC magmatic evolution beyond what can be gleaned from either data set alone (Fig. 5b), providing insights into details of open-system processes.

In rocks that formed from magmas that evolved only by closed-system processes, zircon ε_{Hf} should be uniform and statistically identical to initial ε_{Hf} in their host rocks. Variation in zircon ε_{Hf} that exceeds variability that can be explained by analytical uncertainty for a uniform population suggests evolution involving open-system processes. As noted above, a majority of samples other than PST and Alcyone trachyte meet this criterion for identification of open-system processes. Furthermore, in most rocks globally of intermediate to silicic composition, a great majority of Hf resides in zircon; therefore, mean zircon ε_{Hf} should be very close to ε_{Hf} in host rocks. Where this is not the case, it reveals not only the influence of open-system processes, but also that a large fraction of whole-rock Hf is not represented by the analyzed zircon. Either the analyzed zircon population was highly non-representative (an important part of the range of compositions was missed), or much of the Hf in the rock is in other phases and has a distinctly different isotopic composition.

The range of zircon ε_{Hf} in a majority of samples spans the whole-rock ε_{Hf} value and the mean zircon value is close to whole-rock (Fig. 5b). However, in four samples there is a strong apparent mismatch – two magmatic enclaves (one in the Moss porphyry [MPe1], one in the Times porphyry [SCM-27b]), a relatively mafic (trachyandesitic) zone within a composite feldspar porphyry dike (SCM-30), and a post-PST intermediate-composition lava (SIT-2) – in which most or all zircon ε_{Hf} values are either lower or higher than ε_{Hf} of their host whole-rocks. In three cases zircon values are equal to or less than whole-rock, and in the fourth they are equal to or greater than whole-rock (Fig. 5b).

In the magmatic enclaves and feldspar porphyry dike, whole-rock ε_{Hf} exceeds calculated mean zircon ε_{Hf} by ~2 units; ε_{Hf-WR} of -8 to -10 indicates a larger juvenile component than $\varepsilon_{Hf-Zircon}$. For individual zircon analyses in these samples, ε_{Hf} is 0 to 5 units lower than whole-rock. However, the range of ε_{Hf} in magmatic enclave zircons is nearly identical to zircon ε_{Hf} ranges in their respective Times and Moss porphyry host rocks (Fig. 5b). We suggest that enclave zircons are likely xenocrysts entrained from the partially crystallized Times and Moss porphyry host magmas during the injection of more mafic, juvenile material. Similarly, the range of zircon ε_{Hf} in trachyandesitic sample SCM-30 matches the ε_{Hf} range in a more silicic section of the same composite dike (SCM-1b, trachytic), again indicating that the zircon bears the isotopic signature of its original host instead of the more juvenile magma into which it was incorporated. Assuming that our sample set is sufficiently statistically robust, any zircons that grew within the enclaves and dike melts were likely too small to extract via typical mechanical and gravimetric mineral separation methods.

In trachyte lava SIT-2, mean zircon ε_{Hf} exceeds whole-rock ε_{Hf} by ~3 units; the zircon has a more juvenile signature than its more crustal host. SIT-2 is characterized by large, 2-3 cm rounded feldspar glomerocrysts (some with reaction rims), phenocrysts (or xenocrysts) of biotite and sphene with reaction textures, and sparse clinopyroxene and feldspar microlites within a glassy matrix. We surmise that the differences in zircon and whole-rock ε_{Hf} reflect the injection of a more evolved magma into, and the partial resorption of, a less evolved feldspar-rich cumulate. We propose that the analyzed zircon was derived from the disaggregated cumulate, and therefore that its isotopic composition approaches that of the more primitive magma from which the cumulate crystallized; in contrast, the whole-rock composition of SIT-2 reflects that of the injected, more isotopically evolved, magma. The less radiogenic component of whole-rock Hf is probably in large part contained within the glassy matrix (melt).

Proposed Evolution of the SBMVC

We propose the following reconstruction of the SBMVC's magmatic evolution based on whole-rock and zircon isotopic constraints in conjunction with field, elemental and petrographic data (Fig. 6):

(1) ~19 – 18.8 Ma: Eruption of ~10^3 km^3 of intermediate-composition magmas (trachytic and subordinate trachybasaltic and trachyandesitic lavas, Cook Canyon

ignimbrite), all produced from a combination of juvenile, enrichedmantle-derived magma and Paleoproterozoic Mojave crustal material. Relative crustal contributions to pre-PST lavas were variable; Alcyone trachyte at the base of the pre-PST lava section records the greatest crustal contribution of analyzed pre-PST units (Figs. 3 and 4). One pre-PST lava and a PST magmatic enclave provide isotopic evidence for input of magmas with dominantly sources prior to and during the PST episode.

(2) 18.8 Ma: Accumulation, homogenization, and eruption of the >700 km^3 PST magma body. The narrow, relatively crust-rich whole-rock and zircon isotopic signatures in rhyolitic and trachytic PST (Figs. 3, 4, and 5) distinguish PST from all other analyzed units in the SBMVC except for the early Alcyone trachyte lava. The uniformity of zircon isotopic compositions suggests that zircon growth postdated mixing.

(3) 18.8 – 17 Ma: Episodic eruption and intrusion of relatively small volume, elementally and isotopically diverse magmas. Like their magmatic predecessors, post-PST magmas were generated from a combination of enriched mantle- and Paleoproterozoic crust-derived sources. However, they were more isotopically diverse and in general richer in the juvenile component. Intrasample variability in zircon isotopic composition, along with field and petrographic relations, demonstrates open-system processes and suggests that magma recharge periodically reinvigorated the volcanic center, locally disaggregating and assimilating resident crystal mushes or previously crystallized material.

Implications

(1) Elemental and isotopic data for the PST and intracaldera plutons indicate that they are petrogenetically distinct: the caldera intrusions are more isotopically heterogeneous and record

more juvenile input. Plausibly, the plutons may represent mush from the remains of the base of the PST chamber, rejuvenated and contaminated by more juvenile magma, but the data yield no isotopic evidence for a *direct* petrogenetic connection between the intracaldera plutons and the phenocryst-rich trachyte that has been interpreted as erupted PST mush.

These findings are in this regard consistent with those from some other Cenozoic, large-eruption producing volcanic centers (such as Questa caldera in the Southern Rocky Mountain volcanic field – see Tappa et al., 2011) where intracaldera plutons are isotopically and temporally distinct from high-volume erupted material. Either the high-volume eruptions evacuated essentially all magma from the chamber, or any remaining material was subject to post-eruption modification, as suggested here.

(2) Previous studies (e.g., Tappa et al., 2011; Lipman, 2007) have proposed that ignimbrite-producing felsic volcanic centers exhibit characteristic waxing and waning stages correlating with pre- and post-ignimbrite magmatism, respectively. Other studies (e.g., Annen et al., 2015) also document pre-supereruption thermal priming of the crust and post-supereruption diminished magmatic flux. The SBMVC appears to reflect a similar process. Mineral and whole rock isotopic data from the SBMVC reveal that although all SBMVC rocks formed via hybridization between regional enriched mantle magmas and Proterozoic Mojave crust, the supereruptive PST magma body incorporated a larger crustal component and experienced far more thorough hybridization than its magmatic predecessors or successors. This may suggest an increasing thermal flux prior to the PST eruption (consistent with thermal data reported in McDowell et al., 2014 for this system), transferred advectively from the mantle by mafic magmas and leading to more extensive crustal melting during the “waxing” phase of the SBMVC’s history, and the consequent formation a much larger, hotter, more vigorously convecting magma body.

Subsequent diminished mantle flux resulted in abrupt post-PST waning of magmatism. Post-PST volcanic rocks and intrusions have more primitive whole-rock and zircon isotopic compositions than the PST; in the waning stages of magmatic flux within the SBMVC, these isotopic compositions become more primitive through time, indicating a relative increase in the proportion of mantle input to the regional magmatic system.

Increasing mantle fraction in the small-volume magmas was probably a consequence of one or both of two factors: (a) Massive partial melting in the subjacent crust rendered it more refractory after the PST eruption, and hence the crust contributed a greatly reduced mass to ascending post-PST mantle-derived magmas; and/or (b) diminished mantle magma flux after the PST eruption resulted in cooling and greatly reduced melting in the crust, such that the modest amounts of magma that reached the upper crust had incorporated smaller crustal components.

Acknowledgments: We thank Marsha Lidzbarski for her expertise and assistance in collecting the zircon data presented here, and Charles Ferguson (Arizona Geological Survey) for sharing his extensive knowledge of the southern Black Mountains and of field volcanology in general, and for his assistance in collecting representative samples. Jeff Vervoort, Charles Knaack, Diane Wilford, and Scott Boroughs kindly lent their expertise and facilitated our work at the Washington State Radiogenic Isotope and Geochronology Laboratory. Reviewers Lang Farmer and Peter Lipman and Associate Editor Calvin Barnes provided thorough, careful, constructive comments that were very helpful in revising and improving the manuscript. This research was supported by collaborative NSF grants EAR-0409876 and 0911726 (Vanderbilt) and EAR-0409882 and 0911728 (San Jose State).

Figure Captions

Figure 1: (a) Extent of the 18.8 Ma rhyolitic Peach Spring Tuff and location of its source, the Silver Creek Caldera (Ferguson, 2013; Pamukcu, 2013). BR = Basin and Range, CP = Colorado Plateau, CREC = Colorado River Extensional Corridor, SM = Sacramento Mountains, BM = Black Mountains, CM = Cerbat Mountains, HM = Hualapai Mountains, SCC = Silver Creek Caldera. Box shows approximate extent of the Southern Black Mountains Volcanic Center (SBMVC). (b) Map of SBMVC within area of box shown in (a). Sample locations are shown with their unit numbers (*italicized*, following designations in Table 1). Box shows area of (c). BM = Black Mountains, CM = Cerbat Mountains, HM = Hualapai Mountains. (c) Geology and sample locations in the Oatman-Silver Creek area, southern Black Mountains. The Silver Creek caldera and its immediate environs includes intracaldera PST, post-PST intrusions, and pre- and post-PST volcanics (geology from Ferguson et al., 2013).

Figure 2: Whole rock compositions of units in the SBMVC (data from this study plus previously published datasets from the SBMVC: Lang, 2001, Lang et al., 2008; Pearthree et al., 2010; Frazier, 2013; Pamukcu et al., 2013).

Figure 3: Whole rock isotopic compositions of pre- to post-PST SBMVC units (this study); CREC intrusions (Falkner et al., 1995, Bachl et al., 2001, and unpublished Vanderbilt and San Jose State University data). Strontium-neodymium isotopic fields: inferred enriched mantle composition (Feuerbach et al., 1993); Proterozoic and Mesozoic rocks of the region (Bennett & DePaolo, 1987; Miller and Wooden,1994; Allen et al., 1995; Kapp et al., 2002). Lead isotopic

fields for Mojave and Arizona terranes are from Wooden et al. (1988), Wooden & Miller (1990), and Feuerbach et al. (1998).

Figure 4: Plots of zircon and whole rock isotopic data for pre-PST units (left hand side of graphs) to post-PST units (right hand side of graphs). Numbers along the top of the graphs correlate with unit numbers in Table 1, which represent a general time sequence from pre- to post-PST. (a) Oxygen isotopes in zircon. Top graph shows average values and standard deviations; bottom graph shows full range of zircon $\delta^{18}O$ for each sample. Range of mantle zircon ($\delta^{18}O = +5.5 \pm 0.3‰$) shown for comparison. (b) Hafnium isotopes in zircon. Top graph shows average values and standard deviations; bottom graph shows full range of zircon εHf for each sample. (c) Whole rock εNd, εHf, and $^{87}Sr/^{86}Sr_i$ for all SBMVC units.

Figure 5: Zircon oxygen and hafnium isotope data from SBMVC units. (a) Subset of analyses representing paired O and Hf analyses obtained from the same areas in single grains. (b) Whole rock εHf vs. zircon εHf for pre- to post-PST units. Line shows trend of equal whole rock and zircon ε_{Hf}.

Figure 6: Cartoon depicting the magmatic evolution of the SBMVC as indicated by elemental, isotopic, and field data. PMC: Proterozoic Mojave crust component; EM: enriched Mojave lithospheric mantle component.

References Cited

Allen, C.M., Wooden, J.L., Howard, K.A., Foster, D.A., and Tosdal, R.M. (1995) Sources of the Early Cretaceous plutons in the Turtle and West Riverside mountains, California; anomalous Cordilleran interior intrusions. Journal of Petrology, 36, 1675–1700.

Annen, C., Blundy, J.D., Leuthold, J., and Sparks, S.J. (2015) Construction and evolution of igneous bodies: Towards an integrated perspective of crustal magmatism. Lithos, 230, 206-221.

Bachl, C.A., Miller, C.F., Miller, J.S., and Faulds, J.E. (2001) Construction of a pluton: Evidence from an exposed cross-section of the Searchlight pluton, Eldorado Mountains, Nevada. GSA Bulletin, 113, 1213-1228.

Bachmann, O., and Bergantz, G.W. (2004) On the origin of crystal-poor rhyolites: extracted from batholithic crystal mushes. Journal of Petrology, 45, 1565-1582.

Bachmann, O., Miller, C.F., and De Silva, S.L. (2007) The volcanic–plutonic connection as a stage for understanding crustal magmatism. Journal of Volcanology and Geothermal Research, 167, 1-23.

Bachmann, O., and Bergantz, G. (2008) The magma reservoirs that feed supereruptions. Elements, 4, 17-21.

Baertschi, P. (1976) Absolute ^{18}O content of standard mean ocean water. Earth and Planetary Science Letters, 31, 341-344.

Beard, B.L., and Glazner, A.F. (1995) Trace element and Sr and Nd isotopic composition of mantle xenoliths from the Big Pine Volcanic Field, California. Journal of Geophysical Research, 100, 4169–4179.

Bennett, V.C., and DePaolo, D.J. (1987) Proterozoic crustal history of the western United States as determined by neodymium isotopic mapping. Geological Society of America Bulletin, 99, 674-685.

Bindeman, I.N., and Valley, J.W. (2001) Low-$\delta^{18}O$ rhyolites from Yellowstone: magmatic evolution based on analyses of zircons and individual phenocrysts. Journal of Petrology, 42, 1491-1517.

Bindeman, I.N., Watts, K.E., Schmitt, A.K., Morgan, L.A., and Shanks, P. W. (2007) Voluminous low δ18O magmas in the late Miocene Heise volcanic field, Idaho: Implications for the fate of Yellowstone hotspot calderas. Geology, 35, 1019-1022.

Blichert-Toft, J., Chauvel, C., and Albarède, F. (1997) Separation of Hf and Lu for high-precision isotope analysis of rock samples by magnetic sector-multiple collector ICP-MS. Contributions to Mineralogy and Petrology, 127, 248-260.

Blichert-Toft, J., 2008. The Hf isotopic composition of zircon reference material 91500. Chem. Geol. 253, 252–257.

Bouvier, A., Vervoort, J.D., and Patchett, P.J. (2008) The Lu–Hf and Sm–Nd isotopic composition of CHUR: constraints from unequilibrated chondrites and implications for the bulk composition of terrestrial planets. Earth and Planetary Science Letters, 273, 48-57.

Buesch, D.C. (1991) Changes in depositional environments resulting from emplacement of a large-volume ignimbrite. Special Publication - Society of Economic Paleontologists and Mineralogists, 45, 139-153.

Buesch, D.C. and Valentine, G.A. (1986) Peach Springs Tuff and volcanic stratigraphy of the southern Cerbat Mountains, Kingman, Arizona, in Nielson, J.E., and Glazner, A.F., eds., Cenozoic stratigraphy, structure and mineralization in the Mojave Desert: Los Angeles, California State University, 7-14.

Daley, E.E., DePaolo, DJ. (1992) Isotopic evidence for lithospheric thinning during extension; southeastern Great Basin. Geology, 20, 104-108.

Daley, E.E., DePaolo, DJ. (2000) Neodymium isotopes in basalts of the Southwest Basin and Range and lithospheric thinning during continental extension. Chemical Geology, 169, 157-185.

DeWitt, E., Thorson, J.P., and Smith, R.C. (1986) Geology and gold deposits of the Oatman District, northwestern Arizona. U.S. Geological Survey Bulletin, 1857-1, I1-I28.

Drew, D.L., Bindeman, I.N., Watts, K.E., Schmitt, A.K., Fu, B., and McCurry, M. (2013) Crustal-scale recycling in caldera complexes and rift zones along the Yellowstone hotspot track: O and Hf isotopic evidence in diverse zircons from voluminous rhyolites of the Picabo volcanic field, Idaho. Earth and Planetary Science Letters, 381, 63-77.

Ericksen, S.M., Miller, J.S., Miller, C.F., Harper, B.E., and Aggarwal, J.K. (2004) Isotopic constraints on the evolution of felsic magma in the Aztec Wash pluton, Eldorado Mountains, Nevada. Geological Society of America Abstracts with Programs, 36, 8.

Falkner, C.M., Miller, C.F., Wooden, J.L., and Heizler, M.T. (1995) Petrogenesis and tectonic significance of the calc-alkaline, bimodal Aztec Wash pluton, Eldorado Mountains, Colorado River extensional corridor. Journal of Geophysical Research, 100(B7), 10453-10476.

Farmer, G.L., Perry, F.V., Semken, S., Crowe, B., Curtis, D., and DePaolo, D.J. (1989) Isotopic evidence of the structure and origin of subcontinental lithospheric mantle in southern Nevada. Journal of Geophysical Research, 94, 7885-7898.

Faulds, J.E., Feuerbach, D.L., Miller, C.F., and Smith, E.I. (2001) Cenozoic evolution of the northern Colorado River extensional corridor, southern Nevada and northwest Arizona, in Erskine M.C., et al., eds., The geologic transition, High Plateaus to Great Basin – A symposium and field guide: The Makin volume: Utah Geological Association Publication 30, Pacific Section American Association of Petroleum Geologists Publication GB78, p. 239–271.

Faulds, J.E., Smith, E.I., and Gans, P. (1999) Spatial and temporal patterns of magmatism and extension in the northern Colorado River extensional corridor, Nevada and Arizona: A preliminary report. In Cenozoic geology of the northern Colorado River extensional corridor, Nevada and Arizona: Economic implications of extensional segmentation structures: Nevada Petroleum Society, Field Trip Guide, p. 171-183.

Faulds, J.E., Feuerbach, D.L., Reagan, M.K., Metcalf, R.V., Gans, P., and Walker, J.D. (1995) The Mount Perkins block, northwestern Arizona: An exposed cross-section of an evolving, preextensional to synextensional magmatic system. Journal of Geophysical Research, 100, 15249-15266.

Faulds, J.E., Geissman, J.W., and Mawer, C.K. (1990) Structural development of a major extensional accommodation zone in the Basin and Range Province, northwestern Arizona and southern Nevada; Implications for kinematic models of continental extension. Geological Society of America Memoirs, 176, 37-76.

Ferguson, C.A., McIntosh, W.C., and Miller, C.F. (2013) Silver Creek caldera—The tectonically dismembered source of the Peach Spring Tuff. Geology, 41, 3-6.

Feuerbach, D.L., Reagan, M.K., Faulds, J.E., and Walker, J.D. (1998) Lead isotopic evidence for synextensional lithospheric ductile flow in the Colorado River extensional corridor, western United States. Journal of Geophysical Research: Solid Earth (1978–2012), 103(B2), 2515-2528.

Feuerbach, D.L., Smith, E.I., Walker, J.D., and Tangeman, J.A. (1993) The role of the mantle during crustal extension: Constraints from geochemistry of volcanic rocks in the Lake Mead area, Nevada and Arizona. Geological Society of America Bulletin, 105, 1561-1575.

Fisher, C.M., Vervoort, J.D., and DuFrane, S.A. (2014a) Accurate Hf isotope determinations of complex zircons using the “laser ablation split stream” method. Geochemistry, Geophysics, Geosystems, 15, 121-139.

Fisher, C.M., Vervoort, J.D., and Hanchar, J.M. (2014b) Guidelines for reporting zircon Hf isotopic data by LA-MC-ICPMS and potential pitfalls in the interpretation of these data. Chemical Geology, 363, 125-133.

Frazier, W.O. (2013) Petrochemical constraints on generation of the Peach Spring Tuff supereruption magma, Arizona, Nevada, California (Masters thesis, Vanderbilt University).

Galer, S.J.G., and Abouchami, W. (1998) Practical application of lead triple spiking for correction of instrumental mass discrimination. Mineralogical Magazine of America, 62, 491-492.

Gaschnig, R.M., Vervoort, J.D., Lewis, R.S., and Tikoff, B. (2011) Isotopic evolution of the Idaho batholith and Challis intrusive province, northern US Cordillera. Journal of Petrology, 52, 2397-2429.

Gerber, M.E., Miller, C.F., and Wooden, J.L. (1995) Plutonism at the eastern edge of the Cordilleran Jurassic magmatic belt, Mojave Desert, California. In Miller D.M., and Busby, C., (Eds.), Jurassic magmatism and tectonism in the Cordillera, Geological Society of America Special Paper, 299, 351-374.

Glazner, A.F., Nielson, J.E., Howard, K.E., and Miller, D.M. (1986) Correlation of the Peach Springs Tuff, a large-volume Miocene ignimbrite sheet in California and Arizona. Geology, 14, 840-843.

Glazner, A.F., Coleman, D.S., and Bartley, J.M. (2008) The tenuous connection between high-silica rhyolites and granodiorite plutons. Geology, 36, 183-186.

Hawkesworth, C.J., and Kemp, A.I.S. (2006) Using hafnium and oxygen isotopes in zircons to unravel the record of crustal evolution. Chemical Geology, 226, 144-162.

Kapp, J.L , Miller, C.F., and Miller, J.S. (2002) Ireteba pluton, Eldorado Mountains, Nevada: Late, deep-source, peraluminous magmatism in the Cordilleran Interior. Journal of Geology, 110, 649-669.

Kemp, A.I.S., Hawkesworth, C.J., Paterson, B.A., and Kinny, P.D. (2006) Episodic growth of the Gondwana supercontinent from hafnium and oxygen isotopes in zircon. Nature, 439, 580-583.

Kemp, A.I.S., Hawkesworth, C.J., Foster, G.L., Paterson, B.A., Woodhead, J.D., Hergt, J.M., Gray, C.M., and Whitehouse, M.J. (2007) Magmatic and crustal differentiation history of granitic rocks from Hf-O isotopes in zircon. Science, 315, 980-983.

Kemp, A.I.S., Wilde, S.A., Hawkesworth, C.J., Coath, C.D., Nemchin, A., Pidgeon, R.T., Vervoort, J.D., and DuFrane, S.A. (2010) Hadean crustal evolution revisited: new constraints from Pb–Hf isotope systematics of the Jack Hills zircons. Earth and Planetary Science Letters, 296, 45-56.

Lang, N.P., Walker, B.J., Claiborne, L.L., Miller, C.F., Hazlett, R.W., and Heizler, M.T. (2008) The Spirit Mountain batholith and Secret Pass Canyon volcanic center: A cross-sectional view of the magmatic architecture of the uppermost crust of an extensional terrain, Colorado River, Nevada–Arizona: Geological Society of America Field Guide, 11, 187-214, doi:10.1130/2008.fld011(09).

Lang, N. (2001) Evolution of the Secret Pass Canyon volcanic center, Colorado River Extensional Corridor, northwest Arizona. [M.S. Thesis]. Nashville, Tennessee: Vanderbilt University, 114 p.

Le Bas, M J, Le Maitre, R W, Streckeisen, A, and Zanettin, B A. (1986) Chemical classification of volcanic rocks based on the total alkali-silica diagram. Journal of Petrology, 27, 745-750.

Lidzbarski, M.I. (2014) U-Pb Geochronology of the Miocene Peach Spring Tuff Supereruption And Precursor Cook Canyon Tuff, Western Arizona, USA. Master's Theses. Paper 4502. http://scholarworks.sjsu.edu/etd_theses/4502

Lidzbarski, M., Mundil, R., Miller, J.S., and Vasquez, J.A. (2012) Comparing pre- and post-chemical abrasion ages for Miocene Peach Springs Tuff zircon from ID-TIMS and SIMS analyses. AGU Fall Meeting, December 2012.

Lipman, P.W. (1984) The roots of ash flow calderas in western North America: Windows into the tops of granitic batholiths. Journal of Geophysical Research: Solid Earth, 89(B10), 8801-8841.

Lipman, P.W. (2007) Incremental assembly and prolonged consolidation of Cordilleran magma chambers: Evidence from the Southern Rocky Mountain volcanic field. Geosphere, 3, 42–70.

McDowell, S.M., Miller, C.F., Mundil, R., Ferguson, C.A., and Wooden, J.L. (2014) Zircon evidence for a~ 200 ky supereruption-related thermal flare-up in the Miocene southern Black Mountains, western Arizona, USA. Contributions to Mineralogy and Petrology, 168, 1-21.

McDowell, S.M., Miller, C.F., Ferguson, C.A., Fisher, C., Frazier, W.O., Miller, J.S., Mundil, R., Overton, S., and Vervoort, J. (2012) Geochemical insights into the evolution of a supereruptive volcanic center: magmatic precursors and successors of the Miocene Peach Spring Tuff, southern Black Mountains, western AZ. Geological Society of America Abstracts with Programs, 44, 320.

Metcalf, R.V. (2004) Volcanic–plutonic links, plutons as magma chambers and crust–mantle interaction: a lithospheric scale view of magma systems. Transactions of the Royal Society of Edinburgh: Earth Sciences, 95, 357-374.

Metcalf, R.V., Smith, E.I., Walker, J.D., Reed, R.C., and Gonzales, D.A. (1995) Isotopic disequilibrium among commingled hybrid magmas; evidence for a two-stage magma mixing-commingling process in the Mt. Perkins pluton, Arizona. Journal of Geology, 103, 509-527.

Miller, C.F., and Miller, J.S. (2002) Contrasting stratified plutons exposed in tilt blocks, Eldorado Mountains, Colorado River Rift, NV, USA. Lithos, 61, 209-224.

Miller, C.F., and Wooden, J.L. (1994) Anatexis, hybridization and the modification of ancient crust: Mesozoic plutonism in the Old Woman Mountains area, California. Lithos, 32, 111-133.

Miller, J.S., Glazner, A.F., Farmer, G.L., Suayah, I.B., and Keith, L.A. (2000) A Sr, Nd, and Pb isotopic study of mantle domains and crustal structure from Miocene volcanic rocks in the Mojave Desert, California. Geological Society of America Bulletin, 112, 1264-1279.

Mills, R.D., and Coleman, D.S. (2013) Temporal and chemical connections between plutons and ignimbrites from the Mount Princeton magmatic center. Contributions to Mineralogy and Petrology, 165, 961-980.

Morel, M.L.A., Nebel, O., Nebel-Jacobsen, Y.J., Miller, J.S., Vroon, P.Z., 2008. Hafnium isotope characterization of the GJ-1 zircon reference material by solution and laser-ablation MC-ICPMS. Chem. Geol. 255, 231–235.

Murphy, R.T. (2004) Tectono-magmatic interaction and extensional folding in the Union Pass area, northern Colorado River extensional corridor, northwest Arizona. [M.S. Thesis.] Reno, Nevada: University of Nevada, Reno, 150 p.

Murphy, R.T. and Faulds, J.E., 2013, Preliminary Geologic Map of the North Half of the Union Pass Quadrangle, Mohave County, Arizona. Arizona Geological Survey Contributed Map, CM-13-A, 1 map sheet, map scale 1:24,000.

Murphy, R.T., Faulds, J.E., and Hillmeyer, F.L. (2004) Evolution of Miocene extensional fault and fold systems and influence of magmatism in the northern Colorado River extensional corridor, Union Pass area, northwest Arizona. Geological Society of America Abstracts with Programs, 36, 21.

Murphy, R.T., and Faulds, J.E. (2003) Interactions between Tertiary magmatism and extension in the Colorado River Extensional Corridor, Union Pass area, northwestern Arizona. Geological Society of America Abstracts with Programs, 35, 348.

Pamukcu, A.S., Carley, T.L., Gualda, G.A., Miller, C.F., and Ferguson, C.A. (2013) The evolution of the Peach Spring giant magma body: Evidence from accessory mineral textures and compositions, bulk pumice and glass geochemistry, and rhyolite-MELTS modeling. Journal of Petrology, 54, 1109-1148.

Patchett, P.J., and Tatsumoto, M. (1981) A routine high-precision method for Lu-Hf isotope geochemistry and chronology. Contributions to Mineralogy and Petrology, 75, 263-267.

Pearthree, P.A., Ferguson, C.A., Johnson, B.J., and Guynn, J. (2010) Geologic Map and Report for the Proposed State Route 95 Realignment Corridor, Mohave County, Arizona, v. 1: Arizona Geological Survey DGM-65, 5 sheets, 1:24,000 scale, 44 pp.

Prytulak, J., Vervoort, J.D., Plank, T., and Yu, C. (2006) Astoria Fan sediments, DSDP site 174, Cascadia Basin: Hf–Nd–Pb constraints on provenance and outburst flooding. Chemical Geology, 233, 276-292.

Ransome, F.L. (1923) Geology of the Oatman gold district, Arizona: U.S. Geological Survey Bulletin, 743, 58p.

Renne, P.R., Balco, G., Ludwig, K.R., Mundil, R., and Min, K. (2011) Response to the comment by WH Schwartz et al. on "Joint determination of ^{40}K decay constants and ^{40}Ar*/^{40}K for the Fish Canyon sanidine standard, and improved accuracy for ^{40}Ar/^{39}Ar geochronology" by PR Renne et al. (2010). Geochimica et Cosmochimica Acta, 75, 5097-5100.

Renne, P.R., Mundil., R., Balco, G., Min, K., and Ludwig, K.R. (2010) Joint determination of ^{40}K decay constants and ^{40}Ar*/^{40}K for the Fish Canyon sanidine standard, and improved accuracy for ^{40}Ar/^{39}Ar geochronology. Geochimica et Cosmochimica Acta, 74, 5349-5367.

Schoene, B., J. L. Crowley, D. J. Condon, M. D. Schmitz, and S. A. Bowring (2006), Reassessing the uranium decay con- stants for geochronology using ID-TIMS U-Pb data, Geochimica et Cosmochimica Acta, 70, 426–445.

Tappa, M.J., Coleman, D.S., Mills, R.D., and Samperton, K.M. (2011) The plutonic record of a silicic ignimbrite from the Latir volcanic field, New Mexico. Geochemistry, Geophysics, Geosystems, 12, Q10011.

Thorson, J.P. (1971) Igneous petrology of the Oatman district, Mohave County, Arizona (Ph.D. Thesis): University of California – Santa Barbara, 189 p.

Trail, D., Mojzsis, S.J., Harrison, T.M., Schmitt, A.K., Watson, E.B., and Young, E.D. (2007) Constraints on Hadean zircon protoliths from oxygen isotopes, Ti-thermometry, and rare earth elements. Geochemistry, Geophysics, Geosystems, 8(6).

Valley, J.W., Lackey, J.S., Cavosie, A.J., Clechenko, C.C., Spicuzza, M.J., Basei, M.A.S., Bindeman, I.N., Ferreira, V.P., Sial, A.N., King, E.M., Peck, W.H., Sinha, A.K., and Wei, C. S. (2005) 4.4 billion years of crustal maturation: oxygen isotope ratios of magmatic zircon. Contributions to Mineralogy and Petrology, 150, 561-580.

Varga, R.J., Faulds, J.E., Snee, L.W., Harlan, S.S., and Bettison-Varga, L. (2004) Miocene extension and extensional folding in an anticlinal segment of the Black Mountains accommodation zone, Colorado River extensional corridor, southwestern United States. Tectonics, 23, TC1019.

Vervoort, J.D., Patchett, P.J., Blichert-Toft, J., and Albarede, F. (1999) Relationships between Lu-Hf and Sm-Nd isotopic systems in the global sedimentary system. Earth and Planetary Science Letters, 168, 79-99.

Vervoort, J.D., Plank, T., and Prytulak, J. (2011) The Hf-Nd isotopic composition of marine sediments. Geochimica et Cosmochimica Acta, 75, 5903-5926.

Walker Jr, B.A., Miller, C.F., Lowery Claiborne, L., Wooden, J.L., and Miller, J.S. (2007) Geology and geochronology of the Spirit Mountain batholith, southern Nevada: implications for timescales and physical processes of batholith construction. Journal of Volcanology and Geothermal Research, 167, 239-262.

Watts, K.E., Bindeman, I.N., and Schmitt, A.K. (2011) Large-volume rhyolite genesis in caldera complexes of the Snake River Plain: Insights from the Kilgore Tuff of the Heise Volcanic Field, Idaho, with comparison to Yellowstone and Bruneau–Jarbidge Rhyolites. Journal of Petrology, 52, 857-890.

Watts, K.E., Bindeman, I.N., and Schmitt, A.K. (2012) Crystal scale anatomy of a dying supervolcano: an isotope and geochronology study of individual phenocrysts from voluminous rhyolites of the Yellowstone caldera. Contributions to Mineralogy and Petrology, 164, 45-67.

Wooden, J.L., and Miller, D.M. (1990) Chronologic and isotopic framework for early Proterozoic crustal evolution in the eastern Mojave desert region, SE California. Journal of Geophysical Research, 95(B12), 20,133-20,146.

Wooden, J.L., Stacey, J.S., Howard, K.A., Doe, B.R., and Miller, D.M. (1988) Pb isotopic evidence for the formation of Proterozoic crust in the southwestern United States. In Ernst, W. G., (Ed.), Metamorphism and crustal evolution in the western United States. Englewood Cliffs, N.J., Prentice Hall, p. 68-86.

Woodhead, J.D., and Hergt, J.M. (2005) A preliminary appraisal of seven natural zircon reference materials for *in situ* Hf isotope determination. Geostandards and Geoanalytical Research, 29, 183-195.

Young, R.A., and Brennan, W.J. (1974) Peach Springs Tuff: Its bearing on structural evolution of the Colorado Plateau and development of Cenozoic drainage in Mohave County, Arizona. GSA Bulletin, 85, 83-90.

Zimmerer, M.J., and McIntosh, W.C. (2012a) An investigation of caldera-forming magma chambers using the timing of ignimbrite eruptions and pluton emplacement at the Mt. Aetna caldera complex. Journal of Volcanology and Geothermal Research, 245-246, 128-148.

Zimmerer, M.J., and McIntosh, W.C. (2012b) The geochronology of volcanic and plutonic rocks at the Questa caldera: Constraints on the origin of caldera-related silicic magmas. Geological Society of America Bulletin, 124, 1394-1408.

Table 1: Stages of SBMVC Magmatism and Units Analyzed

Stage of SBMVC Magmatism	Character of Magmatism and Magmatic Products	Unit No.	Unit Name	Sample Names* (Ages, where available)
Post-PST Volcanics ***(18.5 – 16.9 Ma[g])***	Compositionally diverse effusive and explosive volcanism	16	Trachyte Lava (Cottonwood)	***SIT-2*** *(17.58±0.05 Ma)[d]*
		13	Felsic Lava Enclave	***SIT-1b***
		12	Felsic Lava	***SIT-1****(18.50±0.16 Ma)[c]*
Post-PST Intrusions ***(18.8 – 18.2 Ma)***	Intermediate to silicic intracaldera intrusive magmatism (Times Porphyry, Moss Porphyry); intrusion of compositionally diverse crosscutting dikes within and in the immediate vicinity of the caldera	15	Mafic Dike	**SCM-26**
		14	Felsic Porphyry Dikes	***SCM-5a*** *(18.21±0.07 Ma)[c], BCD,* **SCM-42**
		11	Feldspar Porphyry Dikes	***SCM-1b*** *(18.65±0.07 Ma)[c], SCM-13, SCM-30*
		10	Times Enclave	***SCM-27b***
		9	Times Porphyry	***TIP-1*** *(18.63±0.08 Ma)[c], SCM-37, SCM-20, SCM-38*
		8	Moss Enclave	***MPe1***
		7	Moss Porphyry	***MP1 (****18.76±0.11 Ma[c]), SCM-6 (18.84±0.15 Ma[c])*
PST ***(18.8 Ma)[a,b]***	PST supereruption, producing phenocryst-rich trachytic intracaldera and proximal outflow tuff and rhyolitic outflow tuff (>700 km^3; covers ~32,000 km^2)	6B	Enclaves in Outflow	**WSWPST1, PST-NY01A**
		6A	Outflow Rhyolite Tuff[e]	**WSWPST-4D, GJPST-1A, WSWPST2a, PST01D**
		5	Intacaldera & Outflow Phenocryst-rich Trachyte Tuff[e]	**PST-SWA-01A, PSTG-1c, *MLPT-5D,* 28556-P1**
Pre-PST Volcanics ***(~19 – 18.8 Ma)***	Thick (up to ~1 km), phenocryst-rich intermediate-composition trachytic effusive magmatism (~10^3 km^3); intermediate composition explosive volcanism (Cook Canyon Tuff); minor intermediate-composition effusive magmatism	4	Trachyte and Trachyandesite Lavas	**PSK-6a, PSK-7, PSK-14, *PST-11***
		3	Cook Canyon Tuff	**WSE-3a,** *MLPT-7a, MLPT-7b*
		2	Gold Road Trachyte[f]	***SCM-41***
		1	Alcyone Trachyte[f]	***SCM-34*** *(19.01±0.26 Ma[c])*

a – Ferguson et al., 2013 (sanidine Ar/Ar).
b – Lidzbarski et al., 2012 (TIMS and SHRIMP zircon U-Pb).
c – McDowell et al., 2014 (TIMS zircon U-Pb).
d – McIntosh & Ferguson, unpublished data (sanidine Ar/Ar).
e – Frazier, 2013; Frazier et al., in prep.
f – Ransome, 1923; Thorson, 1971.
g – Lang, 2001; Lang et al., 2008.
*Samples in **bold**: whole rock isotopic analysis; samples in *italics*: zircon isotopic analysis.

Table 2: Whole Rock Elemental Geochemistry, Southern Black Mountains Volcanic Center

TABLE 2

Sample	SCM-34	SCM-41	WSE-3a	MLPT-7b	PSK-6a[1]	PSK-7	PSK-14	PSTG-1C	PST-SWA01A	MLPT-5D	28556-P1	GJPST-1A	WSWPST-4D
Unit	1	2	3	3	4	4	4	5	5	5	5	6	6
Type	Pre-PST (Alcyone Trachyte)	Pre-PST (Gold Road Trachyte)	Pre-PST (Cook Canyon Tuff)	Pre-PST (Cook Canyon Tuff)	Pre-PST (Esperanza Trachyte)	Pre-PST Lava	Pre-PST Lava	PST Intracaldera Trachyte Fiamma	PST Outflow Trachyte Pumice	PST Outflow Trachyte Pumice	PST Outflow Trachyte Pumice	PST Outflow Rhyolite Pumice	PST Outflow Rhyolite Pumice
Location[2]	*35° 1' 52.2" N*	*35° 1' 51.3" N*	*34° 54' 12.1" N*	*35° 10' 35.2" N*	*34° 58' 36.3" N*	*34° 59' 8.6" N*	*34° 58' 28.1" N*	*35° 2' 54.9" N*	*34 57' 59.5"*	*34 55' 2.0" N*	*34° 54' 14.9" N*	*35° 14' 14.2" N*	*34° 53' 30.7" N*
	114° 27' 17.2" W	*114° 22' 30.5" W*	*114° 19' 27.4" W*	*114° 4' 30.3" W*	*114° 23' 1.5" W*	*114° 23' 44.2" W*	*114° 23' 0.4" W*	*114° 28' 31.8" W*	*114 16' 05.7'*	*114 13' 16.7" W*	*114° 19' 41.4" W*	*114° 22' 13.7" W*	*114° 22' 18.4" W*
Major Oxides, wt%, normalized to 100													
SiO_2	64.35	63.77	66.09	67.45	66.05	58.13	59.08	68.82	64.60	67.85	69.30	72.03	71.94
TiO_2	0.80	0.91	0.76	0.78	0.67	1.03	1.34	0.47	0.59	0.53	0.46	0.36	0.34
Al_2O_3	16.10	16.44	16.04	16.87	17.15	18.29	17.06	16.16	17.28	16.62	15.39	14.74	14.80
Fe_2O_3(t)[3]	4.53	4.70	3.81	3.74	3.20	5.78	6.84	2.24	4.16	3.04	2.65	1.83	1.69
MnO	0.07	0.09	0.07	0.06	0.05	0.08	0.08	0.07	0.08	0.07	0.08	0.04	0.05
MgO	1.51	1.20	1.00	1.42	0.64	3.03	2.92	0.42	0.78	0.53	1.11	0.17	0.35
CaO	3.08	4.19	2.34	1.80	2.28	5.50	4.87	1.29	2.37	1.28	1.65	0.55	0.92
Na2O	3.61	3.60	3.50	2.12	4.23	4.27	3.93	4.00	3.92	3.29	2.69	3.89	3.86
K2O	5.63	4.76	6.18	5.61	5.43	3.38	3.36	6.41	6.07	6.72	6.56	6.32	6.03
P2O5	0.32	0.34	0.20	0.14	0.29	0.50	0.51	0.10	0.14	0.07	0.13	0.06	0.03
(LOI)[4]	*1.94*	*2.62*	*3.22*	*6.29*	*nd*[6]	*nd*[6]	*nd*[6]	*0.74*	*4.20*	*4.67*	*5.56*	*0.89*	*1.46*
(oxide sum)	*98.65*	*97.29*	*96.86*	*93.37*	*97.63*	*97.20*	*96.40*	*96.66*	*93.52*	*93.96*	*94.81*	*99.15*	*98.34*
Trace Elements, ppm													
Sc	8.5	8.4	5.5	6.5	4.4	12.3	15.1	6.1	8.6	8.6	6.8	3.2	3.3
V	60	81	48	44	19	134	123	16	28	20	18	19	9
Ba	2226	1391	1637	1369	1917	1422	1160	1016	2559	560	802	87	59
Rb	135	126	148	171	132	85	104	140	129	127	141	142	162
Sr	590	602	551	398	717	1273	974	199	475	129	185	22	27
Zr	570	360	507	497	376	271	335	576	736	479	608	478	475
Hf	11.1	8.4	12.1	10.5	9.1	6.7	8.3	13.3	13.3	10.2	14.4	11.4	11.8
Y	27	27	24	25	27	23	26	34	26	33	34	47	61
Nb	19.4	22.5	36.4	26.6	27.6	15.6	23.9	21.8	14.3	16.9	31.4	28.3	30.8
Ta	1.1	1.4	1.5	2.0	1.6	0.7	1.4	1.4	1.1	1.3	1.4	2.2	2.3
Ga	21	21	21	21	22	22	22	21	19	20	19	20	20
Cu	12	25	36	8	2	28	20	10	15	10	6	3	2
Zn	91	72	58	69	123	86	82	70	75	65	49	46	49
Pb	29	24	23	22	25	19	21	39	29	31	15	25	25
Th	17.1	19.2	27.5	28.7	12.9	11.8	18.7	19.8	13.3	18.9	22.0	22.2	20.8
U	2.8	3.5	5.0	4.3	2.0	2.7	3.4	4.1	1.9	2.0	2.8	2.8	2.9

Table 2: Whole Rock Elemental Geochemistry, Southern Black Mountains Volcanic Center

TABLE 2

Sample	**SCM-34**	**SCM-41**	**WSE-3a**	**MLPT-7b**	**PSK-6a[1]**	**PSK-7**	**PSK-14**	**PSTG-1C**	**PST-SWA01A**	**MLPT-5D**	**28556-P1**	**GJPST-1A**	**WSWPST-4D**
Unit	**1**	**2**	**3**	**3**	**4**	**4**	**4**	**5**	**5**	**5**	**5**	**6**	**6**
Type	Pre-PST (Alcyone Trachyte)	Pre-PST (Gold Road Trachyte)	Pre-PST (Cook Canyon Tuff)	Pre-PST (Cook Canyon Tuff)	Pre-PST (Esperanza Trachyte)	Pre-PST Lava	Pre-PST Lava	PST Intracaldera Trachyte Fiamma	PST Outflow Trachyte Pumice	PST Outflow Trachyte Pumice	PST Outflow Trachyte Pumice	PST Outflow Rhyolite Pumice	PST Outflow Rhyolite Pumice
La	115	87	103	98	94	91	94	173	133	174	147	108	88
Ce	223	172	198	170	189	179	188	338	236	320	298	202	185
Pr	24.1	18.5	22.0	20.1	20.6	19.9	21.3	35.6	26.9	35.8	32.3	26.7	24.7
Nd	87	66	76	71	74	72	77	106	98	129	112	99	96
Sm	12.7	10.3	11.5	11.0	11.5	11.2	12.4	18.1	13.7	18.8	16.8	20.3	20.8
Eu	2.95	2.14	2.18	1.88	2.75	2.60	2.75	3.14	3.52	2.84	2.66	1.54	1.53
Gd	9.3	7.9	7.6	7.7	7.7	7.3	8.3	10.9	9.0	12.0	11.4	14.1	15.7
Tb	1.10	1.00	0.96	0.93	1.04	0.95	1.09	1.45	1.07	1.39	1.52	2.18	2.50
Dy	5.75	5.36	5.02	4.91	5.49	4.96	5.70	7.60	5.51	7.11	7.58	11.10	13.20
Ho	1.05	1.00	0.94	0.91	1.03	0.92	1.02	1.41	0.98	1.27	1.38	1.96	2.45
Er	2.95	2.84	2.54	2.59	2.66	2.32	2.55	3.93	2.82	3.43	3.81	4.88	6.16
Tm	0.44	0.40	0.37	0.37	0.37	0.32	0.35	0.57	0.40	0.48	0.54	0.73	0.85
Yb	2.81	2.57	2.44	2.39	2.28	1.94	2.08	3.49	2.55	2.98	3.46	3.83	4.79
Lu	0.46	0.41	0.38	0.39	0.35	0.30	0.31	0.50	0.43	0.49	0.54	0.51	0.60

samples PSK-6a, PSK-7, and PSK-14 analyzed by WSU lab; all others by XRAL

1: PSK-6a is from the same lava (Esperanza trachyte) as PSK-11; no elemental analysisis available for PSK-11; 2: NAD83; 3: total Fe as Fe2O3; 4: loss on ignition; 5: total oxides a

2 Whole-Rock Elemental Compositions

Sample	**PST01D**	**WSWPST2A**	**WSWPST1**	**PST-NY01A**	**MP1**	**MPe1**	**SCM-38**	**TIP-1**	**SCM-27b**	**SCM-30**	**SCM-1**	**SIT-1**	**SIT-1b**
Unit	**6**	**6**	**6B**	**6B**	**7**	**8**	**9**	**9**	**10**	**11**	**11**	**12**	**13**
Type	PST Outflow Rhyolite Pumice	PST Outflow Rhyolite Pumice	Magmatic Enclave (PST Rhyolite)	Enclave (PST Rhyolite)	Moss Porphyry	Magmatic Enclave (Moss Porphyry)	(Leuocgranit e)Times Porphyry	Times Porphyry	Magmatic Enclave (Times Porphyry)	Feldspar Porphyry Dike	Feldspar Porphyry Dike	Felsic Lava	Magmatic Enclave (Felsic Lava)
Location [2]	*35° 11' 19.3" N*	*34° 53' 24.4" N*	*34° 53' 43.0" N*	*35° 17' 18.5" N*	*35° 6' 36.9" N*	*35° 6' 35.8" N*	*35° 2' 8.0" N*	*35° 4' 35.7" N*	*35° 4' 7.3" N*	*35° 7' 7.8" N*	*35° 4' 46.7" N*	*35° 2' 34.1" N*	*35° 2' 34.3" N*
	114° 2' 12.6" W	*114° 22' 19.3" W*	*114° 22' 21.9" W*	*115° 13' 38.5" W*	*114° 27' 6.6" W*	*114° 27' 3.0" W*	*114° 27' 23.7" W*	*114° 27' 37.5" W*	*114° 26' 58.2" W*	*114° 26' 2.6" W*	*114° 26' 12.1" W*	*114° 20' 36.2" W*	*114° 20' 36.3" W*
Major Oxide													
SiO_2	75.45	75.12	57.61	69.95	66.83	59.07	77.14	74.13	68.08	61.01	67.74	71.00	56.57
TiO_2	0.20	0.23	1.32	0.48	0.69	1.12	0.17	0.29	0.61	0.85	0.63	0.45	1.14
Al_2O_3	13.14	12.84	16.96	15.53	14.92	16.29	12.21	13.14	15.37	14.85	14.94	14.41	17.14
Fe_2O_3(t) [3]	1.06	1.40	7.48	2.62	4.27	7.02	1.48	2.13	3.94	5.88	3.87	2.63	7.12
MnO	0.07	0.08	0.07	0.08	0.06	0.08	0.04	0.04	0.07	0.09	0.07	0.05	0.09
MgO	0.20	0.20	2.50	0.32	1.49	3.24	0.14	0.26	1.01	5.18	1.21	0.82	3.91
CaO	0.75	0.61	5.41	0.20	2.64	4.93	0.35	0.80	1.63	5.40	2.78	2.28	6.98
Na2O	2.72	3.63	3.50	4.95	3.97	4.15	3.39	3.80	4.72	3.01	3.16	3.54	3.59
K2O	6.39	5.86	4.59	5.82	4.92	3.67	5.08	5.38	4.37	3.45	5.40	4.70	2.95
P2O5	0.03	0.02	0.55	0.05	0.21	0.43	0.00	0.02	0.19	0.28	0.19	0.12	0.49
(LOI) [4]	*3.16*	*0.68*	*1.82*	*1.52*	*2.57*	*3.26*	*0.72*	*0.91*	*2.00*	*5.46*	*3.73*	*2.89*	*2.84*
(oxide sum)	*97.83*	*96.01*	*95.98*	*98.47*	*95.94*	*96.58*	*97.83*	*98.66*	*97.65*	*92.74*	*95.52*	*97.23*	*97.83*
Trace Eleme													
Sc	3.5	3.6	12.2	7.3	7.6	12.5	8.4	8.5	5.5	15.2	14.0	16.4	17.6
V	< 5	<5	109	17	62	121	8	14	35	108	51	36	154
Ba	40	40	1943	30	1175	1287	42	309	1324	823	1059	674	1511
Rb	198	195	96	146	158	107	183	142	142	80	156	156	74
Sr	17	18	1514	11	391	712	39	92	286	504	372	291	1106
Zr	221	257	400	635	261	279	135	257	431	200	298	210	273
Hf	8.8	8.1	9.0	13.7	6.3	6.4	5.0	7.7	9.5	4.7	7.4	5.6	6.2
Y	33	33	31	52	19	21	21	29	21	17	26	22	25
Nb	39.4	21.5	21.5	35.1	17.2	21.4	31.8	27.5	21.1	14.6	23.9	22.1	15.2
Ta	2.5	2.4	1.3	2.1	1.1	1.3	2.0	2.0	1.7	0.8	1.6	1.6	0.8
Ga	20	18	22	28	20	20	17	20	20	18	20	18	23
Cu	2	10	33	6	14	14	4	4	4	71	6	6	35
Zn	50	46	87	97	57	48	37	55	71	70	74	40	84
Pb	24	24	46	21	19	15	27	24	28	16	30	25	10
Th	32.9	24.5	20.3	19.2	16.7	13.0	33.7	26.1	15.2	11.9	19.3	28.5	18.8
U	6.2	4.1	4.2	3.2	2.6	2.4	4.8	3.5	2.2	1.9	3.4	4.6	2.1

Table 2: Whole Rock Elemental Geochemistry, Southern Black Mountains Volcanic Center

2 Whole-Rock Elemental Compositions

Sample	**PST01D**	**WSWPST2A**	**WSWPST1**	**PST-NY01A**	**MP1**	**MPe1**	**SCM-38**	**TIP-1**	**SCM-27b**	**SCM-30**	**SCM-1**	**SIT-1**	**SIT-1b**
Unit	**6**	**6**	**6B**	**6B**	**7**	**8**	**9**	**9**	**10**	**11**	**11**	**12**	**13**
Type	PST Outflow Rhyolite Pumice	PST Outflow Rhyolite Pumice	Magmatic Enclave (PST Rhyolite)	Enclave (PST Rhyolite)	Moss Porphyry	Magmatic Enclave (Moss Porphyry)	(Leuocgranit e)Times Porphyry	Times Porphyry	Magmatic Enclave (Times Porphyry)	Feldspar Porphyry Dike	Feldspar Porphyry Dike	Felsic Lava	Magmatic Enclave (Felsic Lava)
La	70	78	151	159	76	74	48	85	74	55	79	66	117
Ce	124	141	235	236	146	146	88	157	132	110	153	126	184
Pr	13.9	15.6	30.8	37.6	15.6	15.9	7.6	15.8	13.2	11.5	16.1	12.5	24.1
Nd	39	48	104	136	53	57	22	49	44	42	53	42	87
Sm	6.7	8.5	15.8	23.9	8.4	9.3	3.5	8.1	6.6	6.9	8.6	6.7	13.5
Eu	0.567	0.629	3.38	1.41	1.57	2.17	0.22	0.89	1.37	1.55	1.45	1.18	2.66
Gd	5.5	6.5	11.0	14.8	5.8	6.7	3.3	5.9	4.8	5.5	6.4	5.5	9.7
Tb	0.89	1.03	1.20	2.15	0.77	0.94	0.51	0.90	0.69	0.68	0.96	0.74	1.17
Dy	5.20	5.85	5.64	11.50	4.03	4.79	2.97	5.10	3.79	3.45	5.18	3.84	5.43
Ho	1.03	1.19	1.01	2.06	0.78	0.89	0.70	1.05	0.75	0.65	1.04	0.78	0.94
Er	3.17	3.47	2.74	5.78	2.14	2.43	2.27	3.07	2.19	1.86	2.89	2.27	2.71
Tm	0.51	0.55	0.37	0.87	0.31	0.35	0.38	0.47	0.33	0.27	0.43	0.35	0.36
Yb	3.18	3.46	2.35	5.49	2.01	2.20	2.67	3.13	2.26	1.70	2.88	2.40	2.18
Lu	0.47	0.47	0.33	0.86	0.31	0.34	0.44	0.50	0.37	0.27	0.45	0.40	0.34

samples PSI

1: PSK-6a isas analyzed (prior to normalization);6: nd = LOI not

Table 2: Whole Rock Elemental Geochemistry, Southern Black Mountains Volcanic Center

Sample	**SCM-42**	**SCM-5a**	**SCM-26**	**SIT-2**
Unit	**14**	**14**	**15**	**16**
Type	Felsic Dike	Felsic Dike	Mafic Dike	Post-PST (Cottonwood Lava)
Location [2]	*35° 1' 59.3" N*	*35° 2' 55.8" N*	*35° 7' 4.5" N*	*35° 2' 55.9" N*
	114° 22' 40.3" W	*114° 26' 25.6" W*	*114° 26' 18.1" W*	*114° 20' 51.9" W*
Major Oxide				
SiO_2	74.02	79.93	55.28	65.80
TiO_2	0.33	0.09	1.13	0.59
Al_2O_3	14.08	10.03	14.97	16.34
$Fe_2O_3(t)^3$	1.66	1.11	8.70	4.56
MnO	0.02	0.02	0.12	0.09
MgO	0.73	0.21	6.11	0.68
CaO	0.58	0.21	6.32	3.16
Na2O	1.95	0.33	3.61	4.03
K2O	6.58	8.07	3.29	4.46
P2O5	0.04	0.00	0.47	0.29
(LOI) [4]	*2.66*	*0.83*	*3.74*	*0.98*
(oxide sum)	*98.02*	*99.90*	*96.19*	*97.02*
Trace Eleme				
Sc	20.0	18.8	8.5	8.4
V	15	8	150	56
Ba	469	423	1167	1789
Rb	202	337	80	94
Sr	71	65	827	1498
Zr	251	67	248	375
Hf	7.0	3.0	5.9	8.4
Y	25	13	24	18
Nb	28.9	27.7	14.4	15.8
Ta	2.0	2.0	0.8	0.8
Ga	17	10	20	22
Cu	7	6	46	13
Zn	39	11	76	75
Pb	26	13	13	33
Th	29.1	32.7	11.5	25.7
U	4.1	5.7	2.0	3.3

Table 2: Whole Rock Elemental Geochemistry, Southern Black Mountains Volcanic Center

Sample	**SCM-42**	**SCM-5a**	**SCM-26**	**SIT-2**
Unit	**14**	**14**	**15**	**16**
Type	Felsic Dike	Felsic Dike	Mafic Dike	Post-PST (Cottonwood Lava)
La	74	29	74	128
Ce	144	51	149	247
Pr	14.7	4.2	17.0	25.6
Nd	49	12	63	91
Sm	7.8	1.7	10.6	13.4
Eu	0.97	0.16	2.38	2.99
Gd	5.6	1.6	7.7	9.1
Tb	0.80	0.26	1.04	0.91
Dy	4.68	1.63	5.30	4.03
Ho	0.95	0.38	1.00	0.68
Er	2.78	1.36	2.69	1.93
Tm	0.46	0.27	0.38	0.27
Yb	3.00	2.00	2.32	1.74
Lu	0.50	0.36	0.36	0.27

samples PSI

1: PSK-6a is

TABLE 3 Whole-rock Isotopic Compositions (Pb, Nd, Hf, Sr)

Sample Name	Unit #	Unit	Pb						Nd				Hf				Sr			
			$^{206}Pb/^{204}Pb$	±	$^{207}Pb/^{204}Pb$	±	$^{208}Pb/^{204}Pb$	±	$^{143}Nd/^{144}Nd$	±	εNd[a]	2SE	$^{176}Hf/^{177}Hf$	±	εHf[b]	2SE	$^{87}Sr/^{86}Sr$[c]	±	$^{87}Rb/^{86}Sr$	$^{87}Sr/^{86}Sr_{Initial}$
SIT-2	16	Post-PST (Cottonwood Lava)	18.4259	0.0038	15.6134	0.0032	39.1487	0.0075	0.512104	14	-10.3	0.3	0.282414	6	-13.1	0.2	0.709818	8	0.177	0.709771
SCM-26	15	Mafic Dike	18.4916	0.0023	15.6248	0.0022	39.2864	0.0053	0.512104	13	-10.3	0.3	0.282450	6	-11.8	0.2	0.710188	10	0.273	0.710115
SCM-5a	14	Felsic Dike	18.3573	0.0039	15.6065	0.0033	39.2777	0.0077	0.512171	14	-9.0	0.3	0.282510	6	-9.7	0.2	0.715932	8	14.636	0.712024
SCM-42	14	Felsic Dike	18.3134	0.0023	15.6104	0.0022	39.1214	0.0054	0.512155	13	-9.3	0.3	0.282479	6	-10.8	0.2	0.713239	8	8.032	0.711095
SIT-1b	13	Magmatic Enclave (Felsic Lava)	18.3176	0.0023	15.6029	0.0022	38.9525	0.0054	0.512157	13	-9.2	0.3	0.282501	6	-10.0	0.2	0.709176	8	0.189	0.709126
SIT-1	12	Felsic Lava	18.2477	0.0027	15.6033	0.0026	39.1237	0.0061	0.512155	14	-9.3	0.3	0.282498	6	-10.2	0.2	0.710537	16	1.513	0.710133
SCM-1	11	Feldspar Porphyry Dike	18.2755	0.0027	15.6019	0.0026	39.0810	0.0061	0.512143	14	-9.5	0.3	0.282487	6	-10.5	0.2	0.710462	8	1.184	0.710146
SCM-30	11	Feldspar Porphyry Dike	18.2449	0.0023	15.5986	0.0022	39.0085	0.0054	0.512194	12	-8.5	0.2	0.282536	6	-8.8	0.2	0.709579	10	0.448	0.709460
SCM-27b	10	Magmatic Enclave (Times Porphyry)	18.3021	0.0038	15.6048	0.0032	39.0608	0.0077	0.512208	14	-8.2	0.3	0.282535	6	-8.8	0.2	0.710034	8	1.402	0.709660
TIP-1	9	Times Porphyry	18.2894	0.0038	15.6087	0.0032	39.1201	0.0075	0.512134	14	-9.7	0.3	0.282456	6	-11.6	0.2	0.711322	8	4.357	0.710158
SCM-38	9	(Leuocgranite)Times Porphyry	18.2842	0.0039	15.6049	0.0032	39.0954	0.0077	0.512126	14	-9.8	0.3	0.282450	6	-11.8	0.2	0.715925	8	13.246	0.712388
MPe1	8	Magmatic Enclave (Moss Porphyry)	18.2864	0.0039	15.6064	0.0033	39.1196	0.0078	0.512197	14	-8.4	0.3	0.282511	6	-9.7	0.2	0.710422	6	0.424	0.710309
MP1	7	Moss Porphyry	18.2692	0.0038	15.6062	0.0032	39.1173	0.0076	0.512104	15	-10.3	0.3	0.282446	6	-12.0	0.2	0.711181	6	1.141	0.710876
PST-NY01A	6B	Enclave (PST Rhyolite)	18.3723	0.0038	15.6035	0.0032	39.2262	0.0076	0.512256	14	-7.3	0.3	0.282576	6	-7.4	0.2	0.726228	18	37.469	0.716224
WSWPST1	6B	Magmatic Enclave (PST Rhyolite)	18.2610	0.0027	15.5886	0.0026	39.0224	0.0062	0.512215	15	-8.1	0.3	0.282539	6	-8.7	0.2	0.709107	8	0.179	0.709059
WSWPST2a	6	PST Outflow Rhyolite Pumice	18.2859	0.0038	15.6150	0.0031	39.2030	0.0074	0.512045	14	-11.4	0.3	0.282392	6	-13.9	0.2	0.720019	6	30.583	0.711854
PST01D	6	PST Outflow Rhyolite Pumice	18.2600	0.0039	15.6092	0.0033	39.2053	0.0077	0.512039	13	-11.5	0.3	0.282396	6	-13.8	0.2	0.731594	6	32.880	0.722815
WSWPST-4D	6	PST Outflow Rhyolite Pumice	18.2590	0.0022	15.6725	0.0021	39.3266	0.0051	0.512042	13	-11.5	0.3	0.282390	6	-14.0	0.2	0.715762	22	16.938	0.711240
GJPST-1A	6	PST Outflow Rhyolite Pumice	18.2181	0.0022	15.6013	0.0021	39.0842	0.0051	0.512050	13	-11.3	0.3	0.282388	6	-14.0	0.2	0.715661	12	18.221	0.710796
28556-P1	5	PST Outflow Trachyte Pumice	18.2181	0.0022	15.6038	0.0021	39.1400	0.0052	0.512050	12	-11.3	0.2	0.282388	6	-14.0	0.2	0.711795	10	2.152	0.711221
MLPT-5D	5	PST Outflow Trachyte Pumice	18.2317	0.0023	15.6040	0.0021	39.1165	0.0053	0.512047	12	-11.4	0.2	0.282395	6	-13.8	0.2	0.712358	10	2.779	0.711616
PST-SWA-01A	5	PST Outflow Trachyte Pumice	18.2044	0.0038	15.6022	0.0032	39.0985	0.0076	0.512037	15	-11.6	0.3	0.282380	6	-14.3	0.2	0.711454	6	0.767	0.711249
PSTG-1C	5	PST Intracaldera Trachyte Fiamma	18.2584	0.0038	15.6083	0.0032	39.1031	0.0076	0.512047	15	-11.4	0.3	0.282385	6	-14.2	0.2	0.712586	6	1.986	0.712056
PSK-14	4	Pre-PST Lava	18.4513	0.0028	15.6173	0.0026	39.1675	0.0062	0.512212	14	-8.2	0.3	0.282552	6	-8.2	0.2	0.709334	10	0.300	0.709254
PSK-7	4	Pre-PST Lava	18.4072	0.0028	15.6157	0.0026	39.1719	0.0062	0.512083	14	-10.7	0.3	0.282415	6	-13.1	0.2	0.710075	10	0.188	0.710025
PST-11[d]	4	Pre-PST (Esperanza Trachyte)	18.3476	0.0022	15.6089	0.0022	39.0053	0.0051	0.512193	14	-8.5	0.3	0.282502	6	-10.0	0.2	0.709442	14	0.521	0.709303
WSE3a	3	Pre-PST (Cook Canyon Tuff)	18.2833	0.0038	15.6050	0.0033	39.0605	0.0081	0.512122	12	-9.9	0.2	0.282465	6	-11.3	0.2	0.710378	10	0.758	0.710175
SCM-41	2	Pre-PST (Gold Road Trachyte)	18.3754	0.0038	15.6149	0.0032	39.1828	0.0075	0.512127	14	-9.8	0.3	0.282461	6	-11.5	0.2	0.710524	8	0.591	0.710367
SCM-34	1	Pre-PST (Alcyone Trachyte)	18.1867	0.0028	15.5984	0.0027	39.0465	0.0066	0.512041	14	-11.5	0.3	0.282390	6	-14.0	0.2	0.711154	8	0.646	0.710982

[a] *εNd calculated using present day CHUR- $^{143}Nd/^{144}Nd$=0.512638 (Bouvier et al., 2008)*

[b] *εHf calculated using present day CHUR- $^{176}Hf/^{177}Hf$=0.282785 (Bouvier et al., 2008)*

[c] *Ratios calculated from ICP-MS trace element data.*

[d] *Sample from same unit as PSK-6a in Table 2 (no elemental analysis available for PST-11); location: 34° 58' 50.0" N, 114° 23' 23.0" W*

Analysts: S.M. McDowell, W.O. Frazier, and C.M. Fisher

TABLE 4 Proterozoic Zircon (U-Pb ages, Hf and O isotopic compositions)

Rock unit and analysis number	U age (Ma)	1 s	U age (Ma)	1 s	^{207}Pb/^{206}Pb age (Ma)	1 s	present day eHf	d^{18}O
Gold Road Trachyte								
SCM41_4	1636	18	1618	28	1676	16	-30	7.9
SCM41_5	1607	18	1509	26	1752	15	-30	5.7
Peach Spring Tuff								
MLPT5D_11	1569	15	1520	22	1664	12	-33	nd
Moss Porphyry								
SCM6_7	1638	19	1611	30	1687	15	-33	nd
MPe1Ne_9	1689	20	1714	31	1673	22		nd
Feldspar Porphyry Dike								
SCM30_22	1636	17	1593	26	1699	14	-33	nd

Table 5 Paired O and Hf isotopic analyses of Zircon

Pre-PST Trachyte - Alcyone	**eHf**	**d^{18}O**
SCM34_1_20	-12.3	6.6
SCM34_2_19	-13.9	6.8
SCM34_4_18	-14.4	6.3
SCM34_5_11	-14.5	7.2
SCM34_11_7	-13.2	6.8
SCM34_10_4	-14.0	6.6
SCM34_1_8	-12.3	6.6
Pre-PST Trachyte - Gold Ro	**eHf**	**d^{18}O**
SCM41_1_1	-10.6	5.9
SCM41_4_3	-29.7	7.9
SCM41_5_2	-29.7	5.7
SCM41_8_7	-13.3	6.4
SCM41_9_6	-10.5	5.7
SCM41_12_12	-12.1	6.6
SCM41_13_11	-11.2	6.4
SCM41_10_10	-13.6	5.7
Cook Canyon Tuff	**eHf**	**d^{18}O**
MLPT7A_1_10	-11.6	6.5
MLPT7A_2_7	-11.6	6.2
MLPT7B_9_1	-10.0	6.4
MLPT7B_7_9	-11.8	6.4
MLPT7B_4_15	-12.1	6.1
MLPT7B_1_10	-11.4	6.3
MLPT7B_2_18	-13.3	6.5
Peach Spring Tuff Rhyolite	**eHf**	**d^{18}O**
MLPT2H_11_3	-13.2	6.4
MLPT2H_9_11	-13.4	6.1

Peach Spring Tuff Trachyte	**eHf**	**d^{18}O**
MLPT5D_9_11	-14.1	6.9
MLPT5D_10_10	-13.8	6.7
MLPT5D_14_9	-13.8	6.1
MLPT5D_15_8	-13.5	6.7
Moss Porphyry	**eHf**	**d^{18}O**
SCM6_1_1	-13.3	6.2
SCM6_7_12	-33.4	6.9
MP1_1-1	-15.2	7.1
MP1_9_13	-10.5	6.1
MP1_1_16	-10.5	6.2
MPe1Ne_1_2	-10.0	6.6
MPe1Ne_18_12	-11.0	6.5
MPe1ne_17_16	-12.8	6.2
MPe1Ne_5_17	-13.2	6.4
MPe1Ne_7_21	-12.5	6.1
MPene1_1_2	-10.0	6.6
Moss Porphyry enclave	**eHf**	**d^{18}O**
MPe1_10_12	-13.9	6.2
MPe1_14_16	-33.3	6.6
Times Granite	**eHf**	**d^{18}O**
SCM20_1_1	-10.4	6.3
SCM20_2_3	-9.8	6.0
SCM20_4_7	-8.5	6.4
SCM20_6_14	-11.7	6.0
SCM20_8_16	-10.2	6.0
SCM20_9_19	-9.9	6.5
SCM20_10_20	-11.4	6.5

MLPT2H_7_15	-15.7	6.5	SCM20_12_28	-10.5	6.1
MLPT2H_8_10	-13.4	6.2	TIP1_3_1	-10.0	5.8
MLPT2H_6_19	-14.5	6.3	TIP1_5_3	-12.3	5.5
MLPT3B_12_2	-12.1	6.5	TIP1_6_5	-14.4	6.2
MLPT3B_10_5	-14.5	6.3	TIP1_8_13	-12.1	6.1
MLPT3B_8_6	-14.8	6.6	TIP1_10_27	-12.1	6.2
MLPT3B_5_14	-13.9	6.3	TIP1_12_28	-10.6	5.9
MLPT3B_3_16	-14.3	6.1	SCM37_3_19	-11.2	4.9
MLPT3B_4_15	-14.1	6.3	SCM37_4_20	-12.6	5.2
MLPT3B_1_18	-13.6	6.3	SCM37_5_18	-8.8	4.7
MLPT3B_7_13	-13.1	4.5	SCM37_8_14	-8.6	4.9
Peach Spring Tuff Trachyte	**eHf**	**$d^{18}O$**	SCM37_15_11	-9.9	5.6
MLPT5D_3_19	-15.7	6.8	SCM37_13_1	-11.6	5.8
MLPT5D_5_16	-14.0	6.8	SCM37_4_20	-12.6	5.2

Table 4 continued.

Times Granite enclave	eHf	$d^{18}O$	Felsic Porphyry Dike	eHf	$d^{18}O$
SCM27B_2_2	-10.6	6.0	SCM30_9_10	-11.2	6.0
SCM27B_5_12	-11.1	6.7	SCM30_16_6	-10.0	5.8
SCM27B_6_11	-13.8	6.3	SCM30_11_1	-10.5	5.9
SCM27B_9_17	-10.2	6.1	SCM30_12_2	-10.8	5.6
SCM27B_10_18	-8.9	6.3	SCM30_10_7	-11.0	5.8
SCM27B_1_1	-10.9	5.8	SCM30_20_20	-9.9	5.6
SCM27B_4_6	-10.6	5.8	**Post-PST Felsic Lava**	**eHf**	**$d^{18}O$**
Feldspar Porphyry Dike	**eHf**	**$d^{18}O$**	SIT1_2_1	-11.8	6.1
SCM5A_4_9	-9.1	5.9	SIT1_3_2	-10.8	6.2
SCM5A_5_11	-12.9	6.1	SIT1_4_8	-10.6	5.7
SCM5A_6_12	-8.2	5.7	SIT1_6_9	-9.9	6.1
SCM5A_7_14	-9.1	5.2	SIT1_8_10	-10.8	6.1
SCM5A_8_17	-9.9	5.9	SIT1_11_12	-9.9	6.4
SCM5A_1_1	-11.5	6.0	**Post-PST Felsic Lava enclav**	**eHf**	**$d^{18}O$**

BCD_1_20	-9.2	5.2
BCD_3_14	-9.1	5.0
BCD_4_13	-10.1	4.6
BCD_5_11	-11.3	5.4
BCD_7_9	-9.2	5.6
BCD_12_1	-9.0	6.1
BCD_10_4	-7.9	5.4
BCD_3_14	-9.1	5.0
Felsic Porphyry Dike	**eHf**	**$d^{18}O$**
SCM1B_1_1	-8.8	5.8
SCM1B_3_2	-11.7	6.3
SCM1B_4_3	-10.9	5.8
SCM1B_8_18	-14.3	6.5
SCM1B_10_21	-9.8	6.1
SCM13_2_18	-10.0	5.6
SCM13_6_14	-10.6	5.4
SCM13_7_13	-9.4	5.8
SCM13_8_12	-11.5	5.6
SCM13_11_9	-9.5	5.9
SCM13_13_8	-8.2	5.7
SCM13_12_7	-5.6	5.7
SCM13_14_5	-9.1	6.0
SCM13_15_4	-12.7	5.9
SCM13_16_1	-9.2	5.2
SCM13_4_17	-10.8	5.5
SCM30_21_18	-11.8	5.9
SCM30_19_16	-9.8	5.8

SIT1B_1_2	-12.2	5.7
SIT1B_3_3	-9.5	6.2
SIT1B_4_5	-9.1	6.1
SIT1b_16_10	-9.9	6.3
SIT1b_17_12	-10.2	5.9
SIT1B_9_14	-10.9	6.5
SIT1B_12_18	-11.9	6.1
SIT1B_11_17	-12.3	6.4
SIT1B_14_20	-10.2	6.0
SIT1B_8_13	-9.7	5.8
Post-PST Intermediate Lava	**eHf**	**$d^{18}O$**
SIT2_14_16	-10.9	6.0
SIT2_13_15	-10.3	5.7
SIT2_11_13	-8.6	6.1
SIT2_12_14	-10.3	5.8
SIT2_10_12	-11.2	6.3
SIT2_8_10	-8.4	6.4
SIT2_6_8	-8.3	6.5
SIT2_5_7B	-9.5	6.1
SIT2_4_5	-13.1	5.8
SIT2_3_2	-10.9	5.9
SIT2_2_3	-10.9	5.6
SIT2_1_4	-9.9	5.7

Note: Sample designations follow this protocol: SCM34_"X"_"Y"; where "X" = Hf spot number and "Y" = O spot number in Supplmentary data files; External precision on eHf is 1.5 eHf units (2sd) based onrepeated analyses of well characterized standard, R33 and FC1 (Fisher et al. 2014). External precision for O varied over the course of the analytical sessions from 0.1 to 0.38 (1 sd) based on repeated analyses of standard R33. Complete results including all errors are presented in the Supplementary data files.

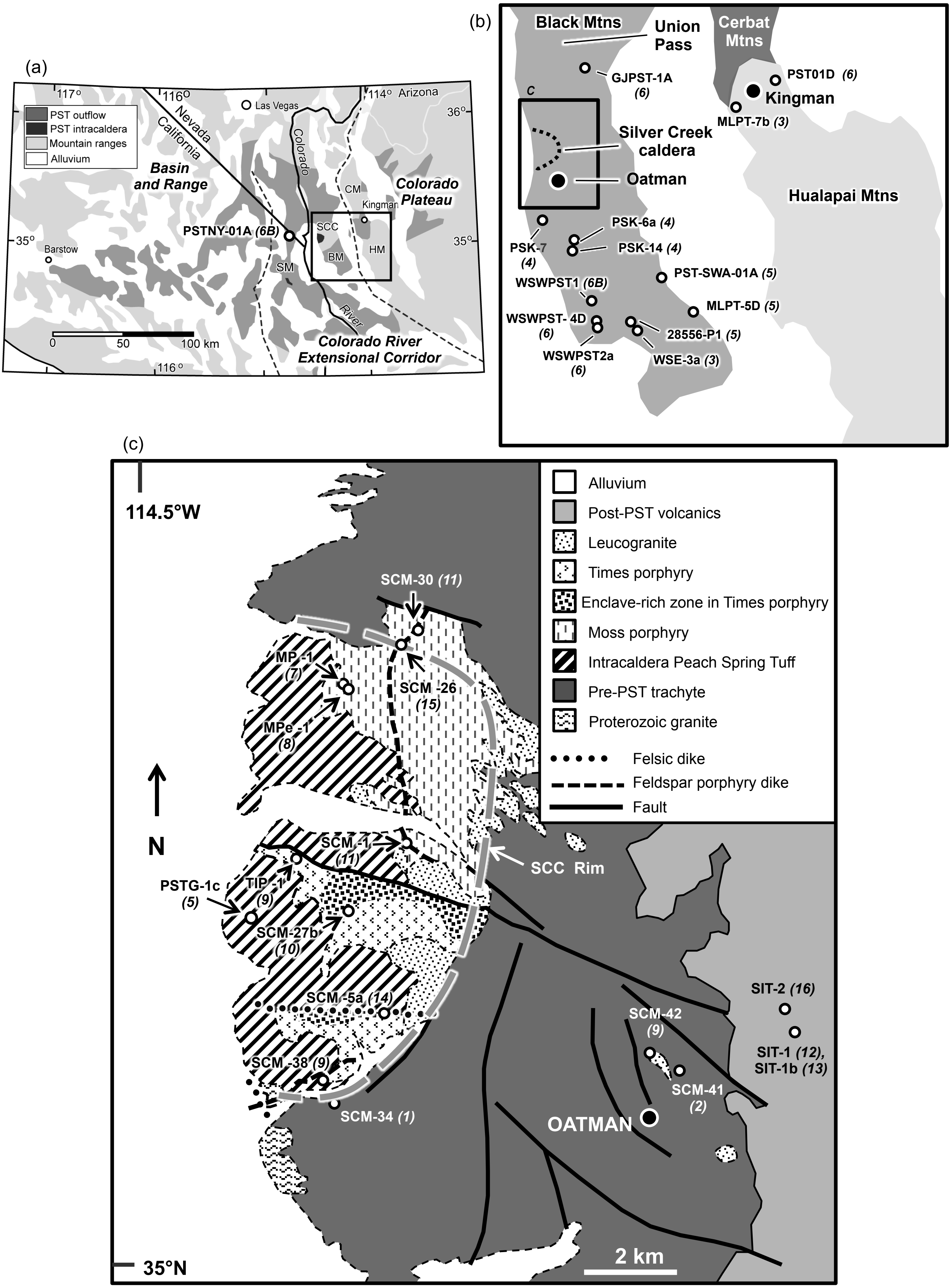

(a)
117°
116°
114°
Arizona
36°
35°
116°
Las Vegas
Nevada
California
Colorado
PST outflow
PST intracaldera
Mountain ranges
Alluvium
Basin and Range
Colorado Plateau
CM
Kingman
SCC
BM
HM
SM
PSTNY-01A (6B)
Barstow
River
Colorado River Extensional Corridor
0
50
100 km
(b)
Black Mtns
Union Pass
Cerbat Mtns
GJPST-1A (6)
PST01D (6)
Kingman
MLPT-7b (3)
c
Silver Creek caldera
Oatman
Hualapai Mtns
PSK-6a (4)
PSK-7 (4)
PSK-14 (4)
PST-SWA-01A (5)
WSWPST1 (6B)
MLPT-5D (5)
WSWPST- 4D (6)
28556-P1 (5)
WSWPST2a (6)
WSE-3a (3)
(c)
114.5°W
Alluvium
Post-PST volcanics
Leucogranite
Times porphyry
Enclave-rich zone in Times porphyry
Moss porphyry
Intracaldera Peach Spring Tuff
Pre-PST trachyte
Proterozoic granite
Felsic dike
Feldspar porphyry dike
Fault
SCM-30 (11)
MP -1 (7)
SCM -26 (15)
MPe -1 (8)
N
SCM -1 (11)
SCC Rim
PSTG-1c (5)
TIP -1 (9)
SCM-27b (10)
SCM -5a (14)
SIT-2 (16)
SCM-42 (9)
SIT-1 (12), SIT-1b (13)
SCM -38 (9)
SCM-41 (2)
SCM-34 (1)
OATMAN
35°N
2 km

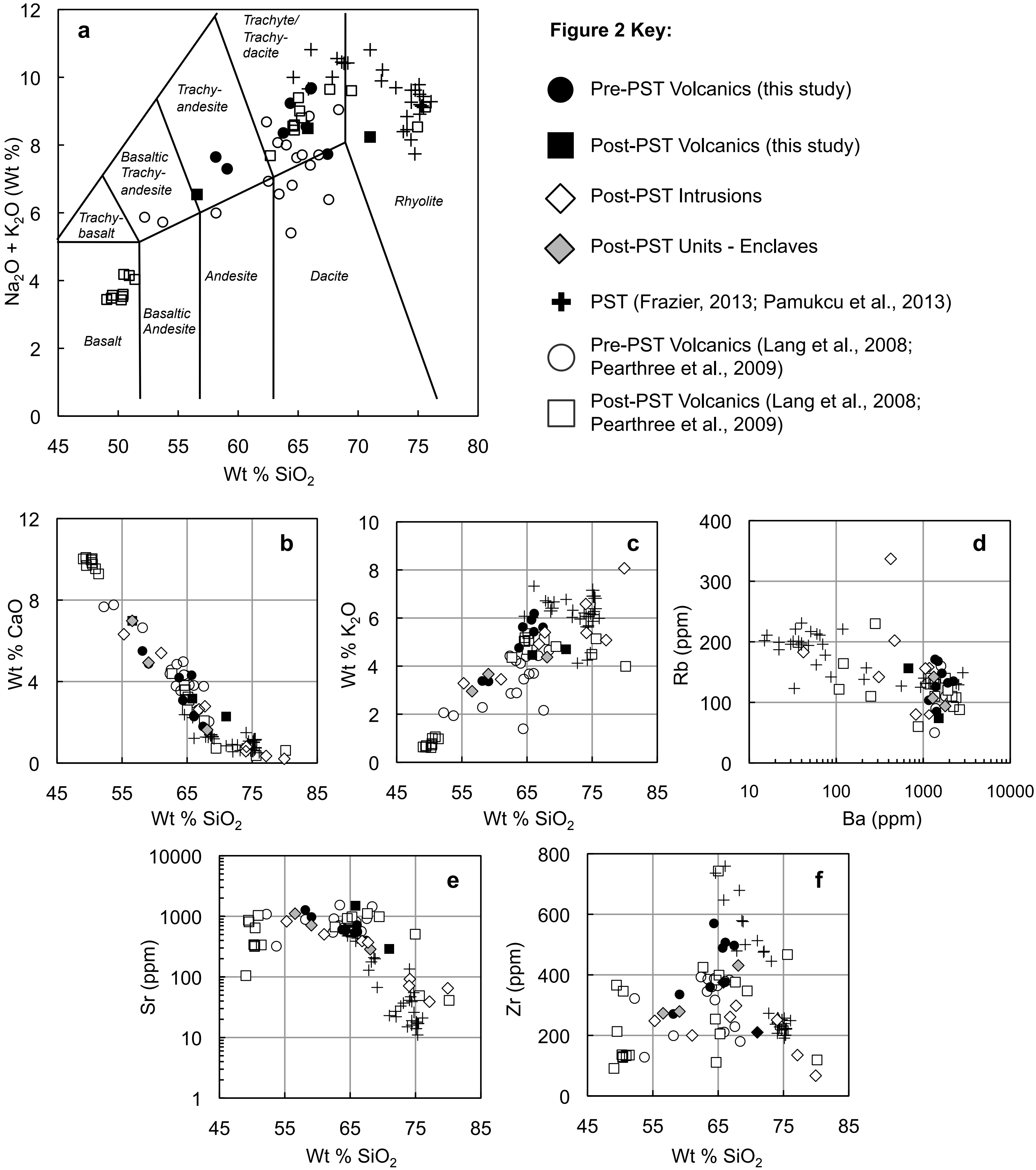

Figure 2 Key:
Pre-PST Volcanics (this study)
Post-PST Volcanics (this study)
Post-PST Intrusions
Post-PST Units - Enclaves
PST (Frazier, 2013; Pamukcu et al., 2013)
Pre-PST Volcanics (Lang et al., 2008; Pearthree et al., 2009)
Post-PST Volcanics (Lang et al., 2008; Pearthree et al., 2009)
a
Trachyte/ Trachy-dacite
Trachy-andesite
Basaltic Trachy-andesite
Trachy-basalt
Rhyolite
Andesite
Dacite
Basaltic Andesite
Basalt
$Na_2O + K_2O$ (Wt %)
Wt % SiO_2
b
Wt % CaO
Wt % SiO_2
c
Wt % K_2O
Wt % SiO_2
d
Rb (ppm)
Ba (ppm)
e
Sr (ppm)
Wt % SiO_2
f
Zr (ppm)
Wt % SiO_2

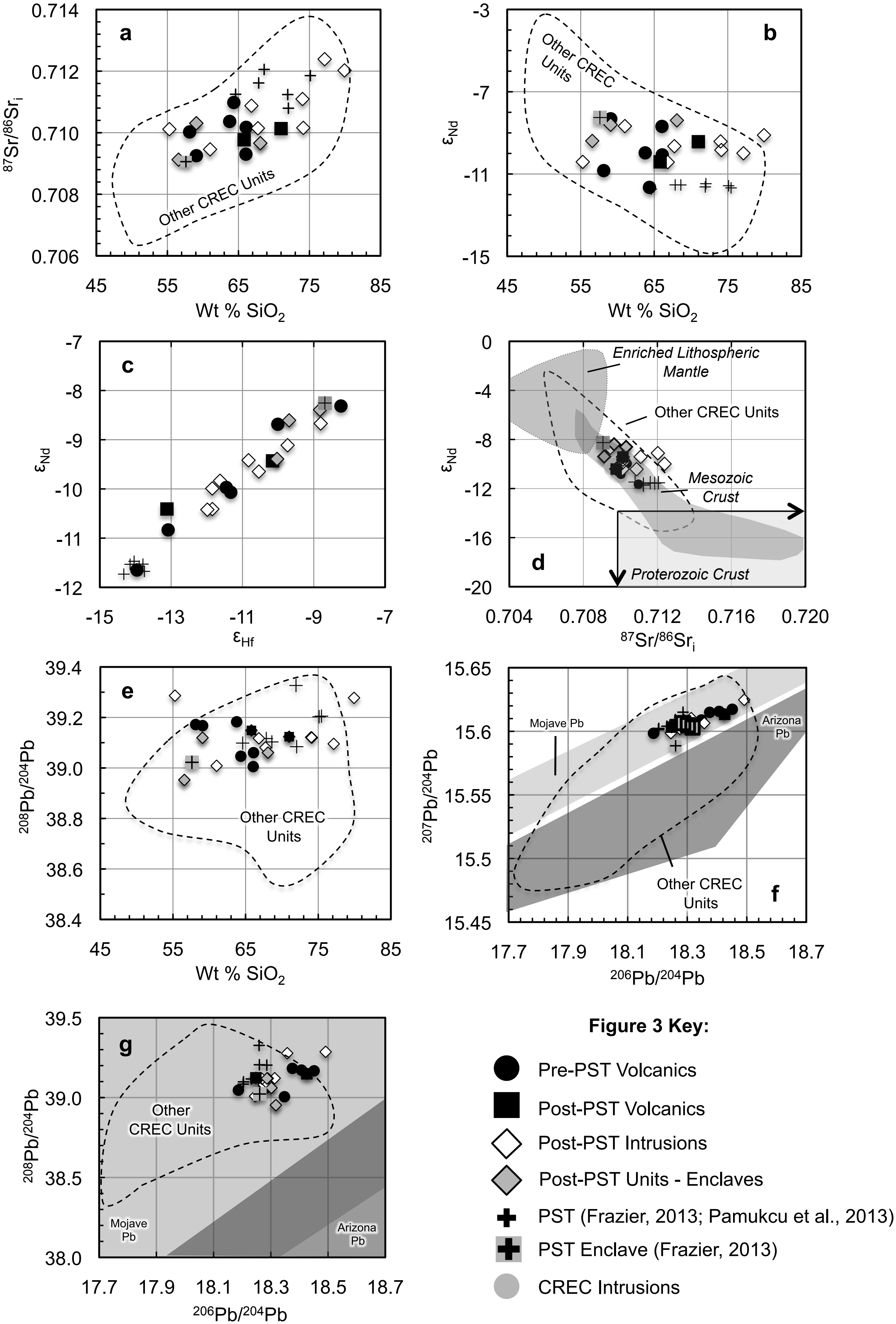

a
$^{87}Sr/^{86}Sr_i$
Other CREC Units
Wt % SiO_2
b
ε_{Nd}
Other CREC Units
Wt % SiO_2
c
ε_{Nd}
ε_{Hf}
d
Enriched Lithospheric Mantle
Other CREC Units
Mesozoic Crust
Proterozoic Crust
ε_{Nd}
$^{87}Sr/^{86}Sr_i$
e
$^{208}Pb/^{204}Pb$
Other CREC Units
Wt % SiO_2
f
Mojave Pb
Arizona Pb
Other CREC Units
$^{207}Pb/^{204}Pb$
$^{206}Pb/^{204}Pb$
g
Other CREC Units
Mojave Pb
Arizona Pb
$^{208}Pb/^{204}Pb$
$^{206}Pb/^{204}Pb$
Figure 3 Key:
Pre-PST Volcanics
Post-PST Volcanics
Post-PST Intrusions
Post-PST Units - Enclaves
PST (Frazier, 2013; Pamukcu et al., 2013)
PST Enclave (Frazier, 2013)
CREC Intrusions

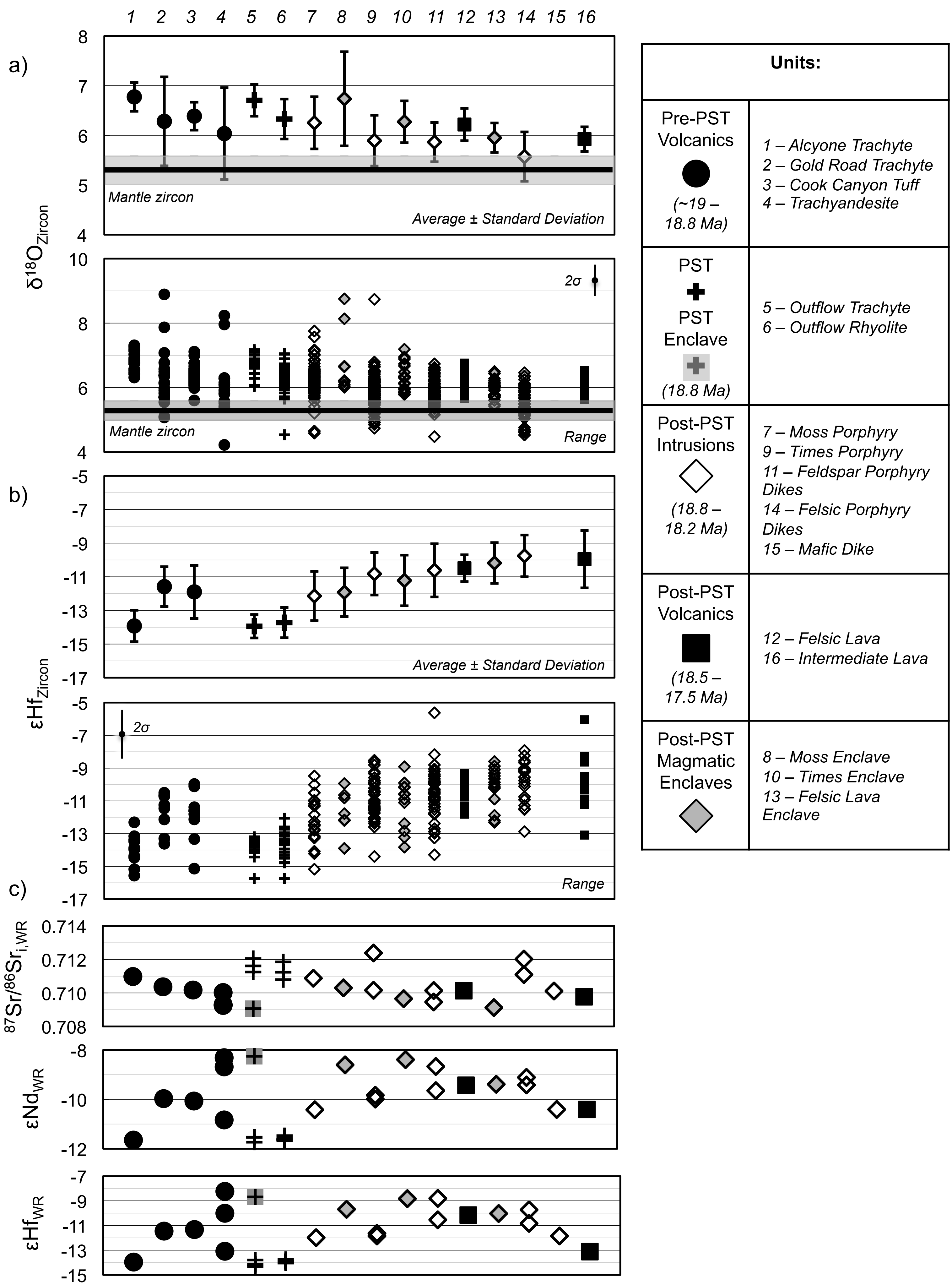
1 2 3 4 5 6 7 8 9 10 11 12 13 14 15 16
a)
δ18OZircon
Mantle zircon
Average ± Standard Deviation
2σ
Range
b)
εHfZircon
c)
87Sr/86Sri,WR
εNdWR
εHfWR
Units:
Pre-PST Volcanics
(~19 – 18.8 Ma)
1 – Alcyone Trachyte
2 – Gold Road Trachyte
3 – Cook Canyon Tuff
4 – Trachyandesite
PST
PST Enclave
(18.8 Ma)
5 – Outflow Trachyte
6 – Outflow Rhyolite
Post-PST Intrusions
(18.8 – 18.2 Ma)
7 – Moss Porphyry
9 – Times Porphyry
11 – Feldspar Porphyry Dikes
14 – Felsic Porphyry Dikes
15 – Mafic Dike
Post-PST Volcanics
(18.5 – 17.5 Ma)
12 – Felsic Lava
16 – Intermediate Lava
Post-PST Magmatic Enclaves
8 – Moss Enclave
10 – Times Enclave
13 – Felsic Lava Enclave

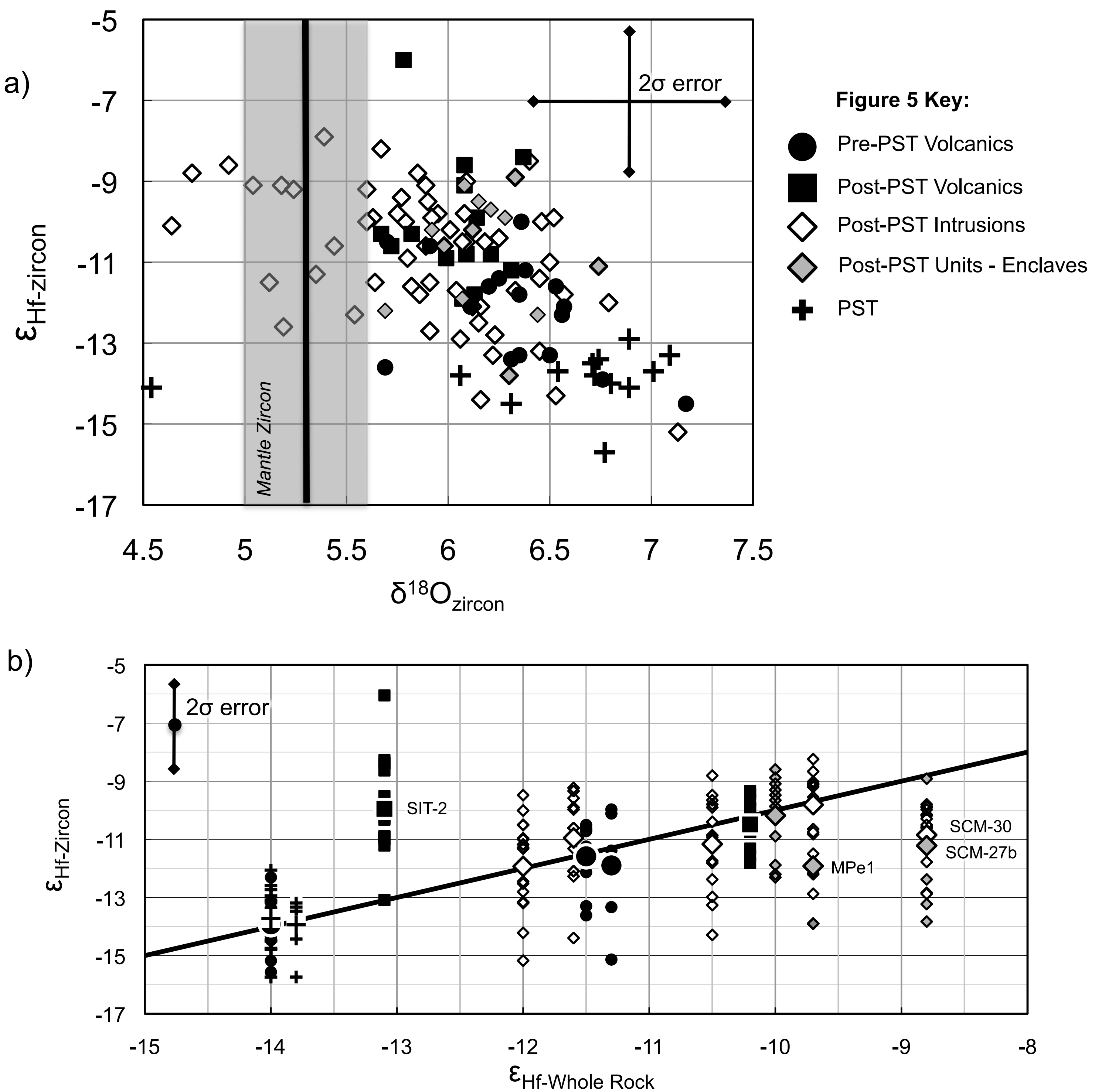

a)
-5
-7
-9
-11
-13
-15
-17
4.5
5
5.5
6
6.5
7
7.5
$\varepsilon_{Hf\text{-}zircon}$
$\delta^{18}O_{zircon}$
Mantle Zircon
2σ error
Figure 5 Key:
Pre-PST Volcanics
Post-PST Volcanics
Post-PST Intrusions
Post-PST Units - Enclaves
PST
b)
2σ error
SIT-2
SCM-30
SCM-27b
MPe1
-15
-14
-13
-12
-11
-10
-9
-8
$\varepsilon_{Hf\text{-}Zircon}$
$\varepsilon_{Hf\text{-}Whole\ Rock}$

1. Pre-PST Magmatism (19 – 18.8 Ma):

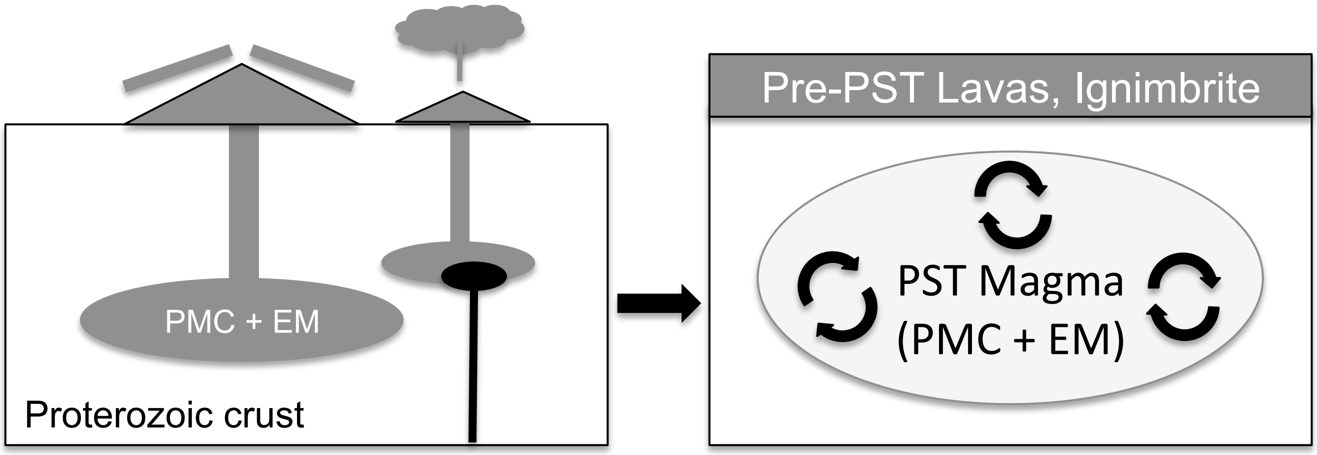

- ~~10^3 km^3 erupted magma
- Dominantly intermediate composition
- Predominantly effusive magmatism; one major explosive eruption (Cook Canyon Tuff)
- Mingling and mixing of PMC and EM components
- Mafic input near time of PST eruption

PST magma body:

- Sources: EM + PMC, with relatively large PMC component
- Rhyolitic upper zone, crystal-rich trachytic lower zone
- Enclaves provide evidence for limited mafic input
- Isotopically well mixed; homogeneous at bulk rock and zircon scales

2. PST Supereruption (18.8 Ma):

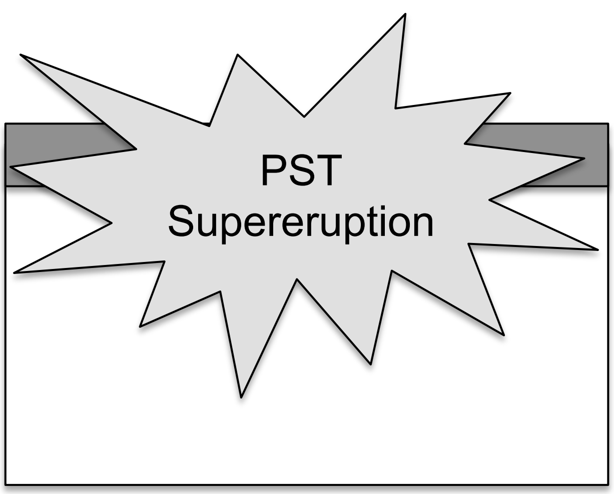

- >700 km^3 D.R.E. erupted
- Areal extent >32,000 km^2
- Only supereruption within the CREC
- Dominated by high-silica rhyolite, lesser low-silica rhyolite and phenocryst-rich trachyte

3. Post-PST Magmatism (18.8 – 17 Ma):

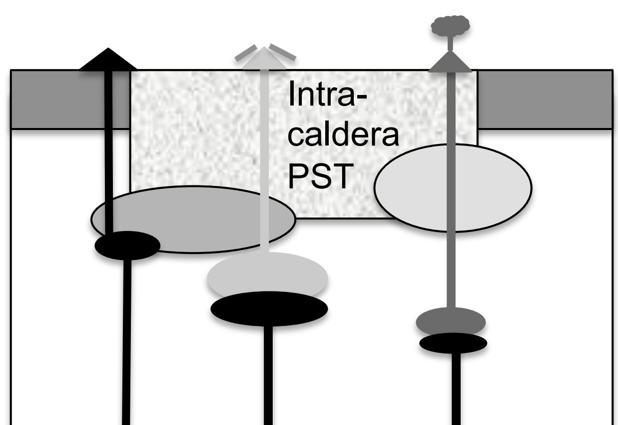

- Periodic eruption, intrusion, crystallization of geochemically diverse, small-volume magmas
- Intracaldera intrusions: petrochemically and genetically distinct from PST
- Sources: EM + PMC, with increasing EM contribution through time